J. Fluid Mech. (2001), *vol.* 437, *pp.* 337–365. Printed in the United Kingdom

On the finite-amplitude steady convection in rotating mushy layers

By PETER GUBA

Department of Geophysics, Faculty of Mathematics and Physics, Comenius University, 842 48 Bratislava, Slovakia

(Received 6 March 2000 and in revised form 12 December 2000)

This study concentrates on a relatively simple model of a mushy layer originally proposed by Amberg & Homsy (1993) and later studied in further detail by Anderson & Worster (1995). We extend this model to the case in which the system is in a state of uniform rotation about the vertical. Of particular interest is to determine how the rotation of the system controls the bifurcating convection with both the oblique-roll planform and the planform of hexagonal symmetry. We find that two-dimensional oblique rolls can be either subcritically or supercritically bifurcating, depending on a pair of parameters $(K_1/C_S, \mathscr{T})$, where K_1 measures how the permeability linearly varies with the local solid fraction, C_S relates the compositional difference between the liquid and solid phases to the variation of composition throughout the mushy layer, and the Taylor number $\mathscr{T}$ gives a measure of the local Coriolis acceleration relative to the viscous dissipation in a porous medium. The three-dimensional convection with hexagonal symmetry is found to be transcritical. Furthermore, distorted hexagons with upflow at the centres can be either subcritical or supercritical, depending on the value of the Taylor number $\mathscr{T}$.

1. Introduction

When a binary alloy solidifies directionally, a flat solidification front can become morphologically unstable owing to constitutional supercooling (see e.g. Porter & Easterling 1992). As a consequence of this supercooling, regions of coexisting liquid and solid phases, referred to as 'mushy' regions, are often formed.

An inevitable feature of the solidification process in the mushy region of binary mixture pertains to the preferential rejection of the lighter component of the mixture into the liquid during solidification. This rejection induces compositional gradients which, in combination with existing temperature gradients and the gravitational field, may induce buoyancy-driven convection within the mushy layer. Convection in mushy layers has received attention in recent years because of its common occurrence in both industrial and geophysical applications, but also since it is interesting as a fluid-dynamics phenomenon as well. A general review of previous works on this problem has been given by Worster (1997).

Most of our understanding of the solidification process via the phase separation within the mushy region is based on laboratory experiments (e.g. Copley *et al.* 1970; Chen & Chen 1991; Tait & Jaupart 1992). Using aqueous solutions of ammonium chloride, analogue systems for binary metallic alloys, it was established that the formation of small imperfections, or 'freckles', is a result of convection through

chimneys in the mushy layer. Chimneys are localized vertical channels of zero solid fraction from which emanate plumes of relatively dilute fluid.

A number of complementary theoretical approaches have been followed to advance the understanding of complex interactions occurring during the solidification of binary alloys. A mathematical model to examine the stability of convective flow in a limiting case involving no interaction between convection and solidification in the mushy layer has been developed by Fowler (1985). Worster (1992) analysed the linear stability of the coupled liquid and mush regions and found two distinct modes of convective instability: one is the boundary-layer mode corresponding to finger-like convection in a compositional boundary layer at the mush-liquid interface, and the other is the mushy-layer mode in which convection is initiated within the mushy layer. The mushy-layer mode of convective instability has been inferred to be a precursor to the formation of chimneys. Emms & Fowler (1994) analysed the linear stability of convection in a model in which the mushy layer was assumed to be of fixed permeability and the convection in the liquid region was supposed to have a finger-like structure. Their analysis implied that the onset of convection in the mushy layer is only slightly influenced by the convection in the liquid region above the mush.

Linear stability analyses allow one to find the critical conditions at which convective instabilities of infinitesimal amplitudes first occur. Nevertheless, it was anticipated (Fowler 1985; Worster 1992) that the mushy-layer mode of convective instability would be subcritically unstable. This issue has been recently confirmed by the analysis of Amberg & Homsy (1993) and studied in further detail by Anderson & Worster (1995). Amberg & Homsy (1993) developed a relatively simple model in which the mushy layer was dynamically isolated from the liquid region above and the solid region below the mushy layer, and the position of mush–liquid interface was taken to be fixed. They performed a weakly nonlinear analysis considering steady convecting states in the mushy layer. Both two-dimensional roll and three-dimensional hexagonal patterns were investigated. Their analysis revealed that the bifurcation to rolls could be either supercritical or subcritical, and the bifurcation to hexagons was always transcritical. Anderson & Worster (1995) extended the analysis of Amberg & Homsy (1993) with a particular interest to determine the stability of steady convecting states in the weakly nonlinear limit. A key finding of their analysis was a set of coupled evolution equations. An analysis of these equations enabled them to reveal the possibility of an oscillatory convective instability in the system, the nature of which was identified and explored in their later paper (Anderson & Worster 1996).

Since freckles are known to reduce the mechanical quality of the final solidified castings, much attention is currently focused on the question of how to avoid their deleterious effects in industrial casting processes. Experiments designed to eliminate the freckle formation have been performed. Sample & Hellawell (1982, 1984) were the first to consider a rotation of the solidifying system, implemented in various ways, as possible means of suppressing freckle formation. In particular, they conducted experiments using NH_4Cl–H_2O and Pb–Sn alloy systems cooled from below to explore the effects of rotation about both inclined and vertical axes, with respect to the orientation of the gravity field. In the case of an inclined rotation axis, they discovered that convection in the form of buoyant plumes emanating from chimneys can be effectively suppressed for certain values of inclination angle and of uniform angular velocity. In contrast, however, they observed no such effect in the case of rotation about the vertical axis; the development of freckles was then essentially identical to that of the non-rotating case. Note that in these experiments, the rotation was present throughout the time of solidification.

More recently, Claßen, Heimpel & Christensen (1999) carried out experiments on an aqueous solution of ammonium chloride in a cylindrical annulus cooled from below. Similarly to Sample & Hellawell (1984), by rotating the base about its vertical axis, they were able to investigate the effects of imposed rotation on the overall behaviour of the system. Their experiments showed that a helical motion of the plumes in the liquid region, which is known to be only slightly developed in the non-rotating case, was strengthened by the presence of rotation, causing the plumes to be oriented nearly horizontally. As a result, the plumes became unstable and broke up into small buoyant blobs rising in the melt. Although their aim was primarily to elucidate the effect of rotation within the liquid region above the mushy layer, they concluded also, like Sample & Hellawell (1984), that chimney convection within the mushy layer was little affected by the presence of rotation.

The observed experimental facts might lead one to suspect that the rotation about the vertical axis has no effect on chimney convection at all. However, it must be remembered that both studies reported observations relating to strongly nonlinear regimes of chimney convection only; that is, they say nothing about how the rotational constraint, whether with inclined rotation axis or not, affects the onset of chimney convection within the mushy layer. In the present analysis, we shall discover, among other results, how the nonlinear development of steady rotating convection affects the local solid fraction within the mushy layer and draw conclusions regarding the way in which the onset of nonlinear chimney convection can be suppressed, despite the lack of any inclination of the rotation axis.

In this paper, we present an extension of Amberg & Homsy's (1993) study to the case where the mushy layer is in a state of uniform rotation about the vertical. We study the effects of an imposed rotational constraint on the finite-amplitude steady convecting states which arise when the Rayleigh number is slightly in excess of its critical value. In particular, the case of two-dimensional convection in the form of oblique rolls, and the case of three-dimensional convection with hexagonal symmetry are considered. We wish to establish how the qualitative results relating to effects of non-symmetries (see Amberg & Homsy 1993; Anderson & Worster 1995) in the system are altered by the presence of rotation, by identifying the explicit functions of the rotation rate which determine the nature of bifurcations to finite-amplitude convection. We attempt to address the question of particular physical mechanisms through which the rotational constraint manifests itself in the flow at both the linear and weakly nonlinear stages of the system.

The plan of this paper is the following. In § 2, we formulate our problem mathematically and take a particular asymptotic limit of the governing equations in order to carry out calculations explicitly. The weakly nonlinear motions are described by the analysis of § 3, the results of which are divided, for clarity, into the case of two-dimensional convection in the form of oblique rolls and that of three-dimensional convection with hexagonal symmetry. The results are discussed in § 4. Finally, we give some concluding remarks in § 5.

2. Formulation

We consider a physical system in which a mushy layer is held between a completely solid region at the bottom and a completely liquid region at the top (see figure 1). The macroscopic solidification velocity V is assumed to be constant. We adopt the further simplification that the mushy layer is dynamically decoupled from the rest of the system (see Amberg & Homsy 1993; Anderson & Worster 1995) by taking the

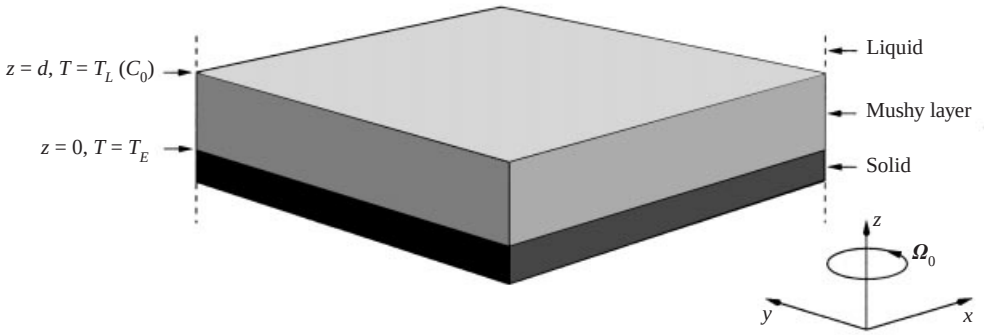

FIGURE 1. A schematic diagram of the mushy layer system. The mushy layer is held between a solid region at the bottom and a liquid region at the top. The top and bottom boundaries of the mushy layer are taken to be isothermal; the boundary $z = 0$ is kept at the eutectic temperature T_E, and the boundary $z = d$ at the liquidus temperature $T_L(C_0)$. The mushy layer is growing at a constant speed V in the vertical direction. The whole system is assumed to be in a state of uniform rotation with angular velocity $\boldsymbol{\Omega}_0$ about the vertical.

top and bottom boundaries of the mushy layer to be impermeable and isothermal. Namely, in a Cartesian frame of reference (x, y, z) moving at the solidification velocity V in the z-direction, the boundary $z = 0$ is kept at the eutectic temperature $T = T_E$, while the boundary $z = d$ is kept at the liquidus temperature $T_L(C_0)$ and is thought to be the surface through which the mixture with composition C_0 is supplied. The solidifying system is assumed to be in a state of rotation at uniform angular velocity $\boldsymbol{\Omega}_0 = \Omega_0 \hat{\boldsymbol{z}}$, where $\hat{\boldsymbol{z}}$ is the vertical unit vector.

The temperature T and composition C of the liquid in the mushy layer are required to satisfy the liquidus relationship $T = T_L(C)$ which is assumed to be linear according to

$$T = T_L(C_0) + \Gamma (C - C_0), \tag{2.1}$$

where Γ is a constant slope of the liquidus curve at $C = C_0$.

The liquid is assumed to be Newtonian with a linearized equation of state

$$\rho_l = \rho_0[1 + \beta(C - C_0)], \tag{2.2}$$

where ρ_0 is a reference density, $\beta = \beta^* - \alpha^* \Gamma$, and α^* and β^* are the constant expansion coefficients for heat and solute, respectively. The compositional effect usually dominates the thermal effect so that β is typically positive and leads to convection driven primarily by compositional buoyancy.

We start with a non-dimensional form of the governing equations which is most similar to that of Worster (1992) and later used by Amberg & Homsy (1993). In this formulation all material properties are assumed to be independent of phase and constant. The dependent variables are scaled as follows. The fluid velocity is scaled with the prescribed solidification velocity V, length and time with the thermal-diffusion lengthscale and timescale, κ/V and κ/V^2, and pressure with $\kappa\mu/\Pi(0)$. Here, κ is the thermal diffusivity, μ is the dynamic viscosity of the liquid and $\Pi(0)$ is the reference value of permeability of the mushy layer. The dimensionless variable for the temperature and concentration is defined by

$$\theta = [T - T_L(C_0)]/\Delta T = (C - C_0)/\Delta C, \tag{2.3}$$

where $\Delta T = \Gamma \Delta C = T_L(C_0) - T_E$, $\Delta C = C_0 - C_E$ and C_E is the eutectic composition.

The dimensionless equations representing the conservation of heat, solute, momentum and mass in the frame of reference which is both translating with the eutectic front and co-rotating with the mushy layer then assume the forms

$$\left(\frac{\partial}{\partial t} - \frac{\partial}{\partial z}\right)(\theta - St\phi) + \boldsymbol{u}\cdot\nabla\theta = \nabla^2\theta, \tag{2.4a}$$

$$\left(\frac{\partial}{\partial t} - \frac{\partial}{\partial z}\right)[(1-\phi)\theta + \mathscr{C}\phi] + \boldsymbol{u}\cdot\nabla\theta = 0, \tag{2.4b}$$

$$K(\phi)\boldsymbol{u} = -\nabla p - Ra\theta\hat{\boldsymbol{z}} + \sqrt{\mathscr{T}}\boldsymbol{u}\times\hat{\boldsymbol{z}}, \tag{2.4c}$$

$$\nabla\cdot\boldsymbol{u} = 0. \tag{2.4d}$$

The dependent variables in these equations are the temperature θ, the local solid fraction ϕ, the Darcy fluid velocity $\boldsymbol{u}$ and the reduced pressure

$$p = [p^* - \tfrac{1}{2}\rho_0\Omega_0^2(x^2+y^2)]\Pi(0)/\kappa\mu,$$

where p^* is the dimensional hydrodynamic pressure of the interstitial fluid in the non-rotating system. The function $K(\phi)$ in equation (2.4*c*) stands for the variations of permeability Π with the local solid fraction ϕ and is defined by $K(\phi) = \Pi(0)/\Pi(\phi)$. We shall follow Worster (1992) in assuming such a constitutive expression for $\Pi(\phi)$ in which the permeability remains finite as the solid fraction approaches zero (see equation (2.15) below).

The dimensionless parameters introduced in the governing equations (2.4) are the Stefan number, the concentration ratio, the Rayleigh number and the Taylor number,

$$St = \frac{\mathscr{L}}{c_l\Delta T}, \quad \mathscr{C} = \frac{C_S' - C_0}{C_0 - C_E}, \quad Ra = \frac{\beta\Delta C g\Pi(0)}{\nu V}, \quad \mathscr{T} = \left(\frac{2\Omega_0\Pi(0)}{(1-\phi_0)\nu}\right)^2, \tag{2.5a–d}$$

respectively, where $\mathscr{L}$ is the latent heat of fusion, c_l is the specific heat, C_S' is the composition of solid phase forming the dendrites and g is the acceleration due to gravity. The Stefan number St expresses the importance of the latent heat relative to the specific heat release. The concentration ratio $\mathscr{C}$ represents the compositional contrast between solid and liquid phases compared to the characteristic variation of composition across the mushy layer. Note that, as we shall consider later, $\mathscr{C}$ will become large if the initial composition C_0 is close to the eutectic composition C_E. The Rayleigh number Ra relates the destabilizing effect of compositional buoyancy to the stabilizing influence of viscous dissipation in the porous medium. The Taylor number $\mathscr{T}$ measures the ratio of the local Coriolis acceleration associated with the imposed rotation relative to the viscous dissipation in the mushy layer. We fix the local solid fraction at a constant value ϕ_0 in the term modelling the effect of rotation, where ϕ_0 is thought of as a reference value of the local solid fraction in the mushy layer (cf. a definition of the Taylor number in the context of rotating convection in passive porous media considered by e.g. Nield & Bejan 1999; Nield 1999 and particularly Vadasz 1998*a*, *b*). Note that this does preclude the possibility of a further nonlinear interaction between perturbations to the local solid fraction and convection associated with the Coriolis term; to follow this demands an enhanced computing requirement. In order to systematically isolate and understand specific key interactions present in the system, it seems sensible at this stage to address the problem with the fixed local solid fraction first.

The imposed dimensionless boundary conditions to be applied to the dependent

variables are

$$\theta = -1, \quad w = 0 \quad \text{at} \quad z = 0, \tag{2.6a,b}$$

$$\theta = 0, \quad w = 0, \quad \phi = 0 \quad \text{at} \quad z = \delta, \tag{2.7a–c}$$

where $\delta = d/(\kappa/V)$ is the dimensionless thickness of the mushy layer and w is the z-component of the fluid velocity $\boldsymbol{u}$. Conditions (2.6) express that the temperature is equal to its eutectic value and the vertical component of the flow is zero on the bottom boundary of the mushy layer $z = 0$. Conditions (2.7) state that the temperature is equal to the liquidus temperature at the initial composition, the vertical component of the flow is zero and the solid fraction is continuous on the top boundary of the mushy layer $z = \delta$. For a more detailed discussion of the merits of these boundary conditions the reader is referred to Anderson & Worster (1995).

Following Amberg & Homsy (1993), we study a limit in which the system is close to the eutectic point by letting $\mathscr{C} = C_S/\delta$ with $C_S = O(1)$ as $\delta \to 0$, where we assume that the thickness of the mushy layer is much less than the diffusive lengthscale. Further, we assume that the Stefan number $St = O(1)$ as $\delta \to 0$. Physically, this corresponds to the situation where the latent heat of solidification is comparable to the heat associated with the typical variations of temperature within the mushy layer.

In the present analysis, we wish to include the effects of the rotational constraint imposed on the system, and therefore have to relate the order of magnitude of the Coriolis force term to the rest of the terms appearing in the momentum equation (2.4c). For this purpose we consider the particular asymptotic limit where

$$\sqrt{\mathscr{T}} = O(1) \quad \text{as} \quad \delta \to 0, \tag{2.8}$$

which, together with the particular rescalings of the problem introduced below, will imply that the Coriolis force is a part of the dominant momentum balance between the pressure gradient, and the buoyancy and Darcy forces. This is, in fact, our motivation for taking the above assumption ($\delta \to 0, \sqrt{\mathscr{T}} = O(1)$). We note that for the ammonium-chloride–water system, if the characteristic value of the permeability $\Pi(0) = 2.31 \times 10^{-3}\,\mathrm{cm}^2$ (Tait & Jaupart 1992) and the kinematic viscosity $\nu = 0.95 \times 10^{-2}\,\mathrm{cm}^2\,\mathrm{s}^{-1}$ (Emms & Fowler 1994) are considered, this limit can be accomplished by values of the angular velocity Ω_0 about 2 $\mathrm{rad\,s}^{-1}$ (with ϕ_0 set to zero in anticipation of considering the limit of small δ).

Analysis of the control balances in equations (2.4) for these asymptotic limits then indicates the following rescalings of the problem

$$(x, y, z) = \delta(\bar{x}, \bar{y}, \bar{z}), \quad R^2 = \delta Ra, \tag{2.9a,b}$$

$$\theta = \theta_B(\bar{z}) + \epsilon\hat{\theta}(\bar{x}, \bar{y}, \bar{z}), \tag{2.9c}$$

$$\phi = \phi_B(\bar{z}) + \epsilon\hat{\phi}(\bar{x}, \bar{y}, \bar{z}), \tag{2.9d}$$

$$\boldsymbol{u} = \boldsymbol{0} + \epsilon\frac{R}{\delta}\hat{\boldsymbol{u}}(\bar{x}, \bar{y}, \bar{z}), \tag{2.9e}$$

$$p = Rp_B(\bar{z}) + \epsilon R\hat{p}(\bar{x}, \bar{y}, \bar{z}), \tag{2.9f}$$

where ϵ is a small perturbation parameter to be determined by weakly nonlinear solutions. The subscript B denotes the basic-state solutions which can vary only vertically, and the caret is used for the perturbation variables which can vary in both the horizontal and vertical directions.

The governing equations and boundary conditions for the particular asymptotic limits described above admit steady basic-state solutions which correspond to zero fluid velocity. These solutions can be obtained as series expansions in powers of δ,

yielding the following expressions:

$$\theta_B = -(1-\bar{z}) + \delta\tfrac{1}{2}\bar{z}(1-\bar{z}) + \delta^2\left(-\tfrac{1}{12}\bar{z}(1-\bar{z})(2\bar{z}-1) + \frac{St}{2C_S}\bar{z}(1-\bar{z})\right) + O(\delta^3), \tag{2.10a}$$

$$\phi_B \equiv \delta\bar{\phi}_B = \delta\frac{1}{C_S}(1-\bar{z}) + \delta^2\left(-\frac{1}{C_S^2}(1-\bar{z})^2 - \frac{1}{2C_S}\bar{z}(1-\bar{z})\right) + O(\delta^3). \tag{2.10b}$$

The equation of continuity, (2.4*d*), can be eliminated by introducing the following general representation:

$$\hat{\boldsymbol{u}} = \nabla\times(\nabla\times\hat{\boldsymbol{z}}\hat{\chi}) + \nabla\times\hat{\boldsymbol{z}}\hat{\psi} \equiv \boldsymbol{\xi}\hat{\chi} + \boldsymbol{\zeta}\hat{\psi} \tag{2.11}$$

for the solenoidal velocity field $\hat{\boldsymbol{u}}$, where the symbols $\boldsymbol{\xi}$ and $\boldsymbol{\zeta}$, representing the corresponding vector operators, have been introduced only for notation convenience. Then, restricting our attention to the case of steady convection, the equations governing the perturbations are readily obtained from (2.4*a*, *b*, *c*),

$$\delta\frac{\partial}{\partial\bar{z}}(\hat{\theta} - St\hat{\phi}) + R\frac{\mathrm{d}\theta_B}{\mathrm{d}\bar{z}}\Delta_2\hat{\chi} + \nabla^2\hat{\theta} = \epsilon R(\boldsymbol{\xi}\hat{\chi} + \boldsymbol{\zeta}\hat{\psi})\cdot\nabla\hat{\theta}, \tag{2.12a}$$

$$\delta\frac{\partial}{\partial\bar{z}}\left((1-\delta\bar{\phi}_B)\hat{\theta} - \theta_B\hat{\phi} - \epsilon\hat{\phi}\hat{\theta} + \frac{1}{\delta}C_S\hat{\phi}\right) + R\frac{\mathrm{d}\theta_B}{\mathrm{d}\bar{z}}\Delta_2\hat{\chi} = \epsilon R(\boldsymbol{\xi}\hat{\chi} + \boldsymbol{\zeta}\hat{\psi})\cdot\nabla\hat{\theta}, \tag{2.12b}$$

$$\boldsymbol{\zeta}\cdot[(\boldsymbol{\xi}\hat{\chi} + \boldsymbol{\zeta}\hat{\psi})K(\delta\bar{\phi}_B + \epsilon\hat{\phi})] = \sqrt{\mathscr{T}}\frac{\partial}{\partial\bar{z}}\Delta_2\hat{\chi}, \tag{2.12c}$$

$$\boldsymbol{\xi}\cdot[(\boldsymbol{\xi}\hat{\chi} + \boldsymbol{\zeta}\hat{\psi})K(\delta\bar{\phi}_B + \epsilon\hat{\phi})] = R\Delta_2\hat{\theta} - \sqrt{\mathscr{T}}\frac{\partial}{\partial\bar{z}}\Delta_2\hat{\psi}, \tag{2.12d}$$

where Δ_2 denotes the two-dimensional Laplacian operator in the horizontal plane, $\Delta_2 \equiv \nabla^2 - (\hat{\boldsymbol{z}}\cdot\nabla)^2$. Equations (2.12*c*) and (2.12*d*) for the scalar functions $\hat{\psi}$ and $\hat{\chi}$, respectively, have been obtained by taking the vertical components of the curl and of the $(\mathrm{curl})^2$ of the momentum equation (2.4*c*). The mathematical formulation of the problem is completed by the boundary conditions on the perturbation variables

$$\hat{\theta} = 0, \quad \hat{\chi} = 0 \quad \text{at} \quad \bar{z} = 0, \tag{2.13a, b}$$

$$\hat{\theta} = 0, \quad \hat{\chi} = 0, \quad \hat{\phi} = 0 \quad \text{at} \quad \bar{z} = 1. \tag{2.14a–c}$$

An important feature of the dynamics of the mushy layer is the variation of the permeability with the local solid fraction. Here, since the basic-state solid fraction is of $O(\delta)$ and the perturbations to the solid fraction will also be expected to be small according to the weakly nonlinear theory, we follow Amberg & Homsy (1993) in expanding the function $K(\phi)$ in a regular series for $\phi \ll 1$,

$$K(\phi) = 1 + K_1\phi + K_2\phi^2 + O(\phi^3). \tag{2.15}$$

Note that, with this expression, the particular scalings presented above allow us to treat the problem analytically with the incorporation of the permeability variations as perturbations at higher-order approximations of the perturbation theory. Note also that the coefficient K_1 in equation (2.15) has to be positive in order to ensure the decreasing of the permeability $\Pi(\phi)$ with the increasing solid fraction ϕ.

3. Finite-amplitude steady convection

Following a standard weakly nonlinear method (see e.g. Malkus & Veronis 1958; Busse 1967), our main aim is to derive some fundamental results of the weakly nonlinear theory which are basic to the understanding of the behaviour of perturbations when nonlinear interactions become significant.

We assume that the perturbation variables and the bifurcation parameter can be expanded in powers of ϵ in the forms

$$\hat{\theta} = \theta_1(\bar{x}, \bar{y}, \bar{z}) + \epsilon\theta_2(\bar{x}, \bar{y}, \bar{z}) + O(\epsilon^2), \tag{3.1a}$$

$$\hat{\phi} = \phi_1(\bar{x}, \bar{y}, \bar{z}) + \epsilon\phi_2(\bar{x}, \bar{y}, \bar{z}) + O(\epsilon^2), \tag{3.1b}$$

$$\hat{\chi} = \chi_1(\bar{x}, \bar{y}, \bar{z}) + \epsilon\chi_2(\bar{x}, \bar{y}, \bar{z}) + O(\epsilon^2), \tag{3.1c}$$

$$\hat{\psi} = \psi_1(\bar{x}, \bar{y}, \bar{z}) + \epsilon\psi_2(\bar{x}, \bar{y}, \bar{z}) + O(\epsilon^2), \tag{3.1d}$$

$$R = R_0 + \epsilon R_1 + \epsilon^2 R_2 + O(\epsilon^3). \tag{3.1e}$$

The thickness of the mushy layer δ and the perturbation amplitude ϵ are two small parameters in our analysis. From the formal point of view, an asymptotic relation between these parameters has to be assumed. Referring to Amberg & Homsy (1993), we take a distinguished limit $\delta = \alpha\epsilon$, where $\alpha = O(1)$ as $\epsilon \to 0$. Note that as the Rayleigh number R, or more exactly the originally defined Ra, is an externally given parameter, the expression (3.1e) defines the perturbation amplitude ϵ.

These forms are now substituted into the perturbation equations (2.12) and the coefficients of the terms ϵ^n ($n = 0, 1, \ldots$) are successively equated to zero. There results a set of linear equations for the unknown functions (θ_n, for example) which may be solved sequentially. The full details of the analysis are rather tedious and therefore are not included here. Instead, only the principal results along the way to obtaining the solvability conditions required for the existence of higher-order solutions are recorded. Note that in the present paper we do not address the question of stability of the finite-amplitude convecting states in the mushy layer. Thus, we do not obtain amplitude equations, describing the evolution of small-amplitude convecting states, from the particular solvability conditions; in the present analysis these conditions give directly an adjustment of free parameters appearing in the expansion of the bifurcation parameter R (see e.g. Manneville 1990).

Plainly, the first step in our analysis will be that of investigating the linear stability properties of basic-state solutions (2.10). It is perhaps worth noting here that the resulting linear stability problem, correct to $O(\delta^0)$, will be degenerate. Formally, this indeterminacy is associated with the existence of distinct solutions which correspond to the same eigenvalue of the linear problem. In the analysis presented below, we consider two solutions to the linearized problem of (2.12) corresponding to the convection in the form of two-dimensional oblique rolls and the three-dimensional convection with hexagonal symmetry. By performing the weakly nonlinear analysis we determine the qualitative properties of these steady convecting states beyond the range of validity of the linear stability theory.

3.1. *Two-dimensional convection in the form of oblique rolls*

We first consider the case of two-dimensional solutions to the perturbation equations (2.12) which are independent of $\bar{y}$ and which, to the leading order, correspond to convection in the form of oblique rolls. Note that the flow is two-dimensional in that

the variation of dependent variables with $\bar{y}$ vanishes, despite the existence of all three components of the flow.

The first equations arise from the coefficients of ϵ^0, and correspond to the linear stability problem. The appropriate solutions to these equations take the form

$$\theta_1 = -\sin(\pi\bar{z})\cos(k\bar{x}), \tag{3.2a}$$

$$\phi_1 = -\frac{1}{C_S}\frac{\pi^2+k^2}{\pi}[1+\cos(\pi\bar{z})]\cos(k\bar{x}), \tag{3.2b}$$

$$\chi_1 = \frac{\pi^2+k^2}{R_0k^2}\sin(\pi\bar{z})\cos(k\bar{x}), \tag{3.2c}$$

$$\psi_1 = \sqrt{\mathscr{T}}\frac{\pi(\pi^2+k^2)}{R_0k^2}\cos(\pi\bar{z})\cos(k\bar{x}), \tag{3.2d}$$

where the Rayleigh number R_0 at this order is given by

$$R_0^2 = \frac{1}{k^2}(\pi^2+k^2)[\pi^2(\mathscr{T}+1)+k^2], \tag{3.3}$$

and k is the wavenumber of a particular perturbation in the $\bar{x}$-direction. Minimizing R_0 with respect to k we can readily find the critical Rayleigh number, R_{0c}, and the corresponding wavenumber, k_c. These are given by

$$R_{0c}(\mathscr{T}) = \pi(\sqrt{\mathscr{T}+1}+1), \quad k_c(\mathscr{T}) = \pi(\mathscr{T}+1)^{1/4}, \tag{3.4a,b}$$

respectively, and we fix R_0 and k at these values in our further analysis.

In the non-rotating case, the critical Rayleigh number and its minimizing wavenumber are constant, $R_{0c} = 2\pi$ and $k_c = \pi$. They, as well as the solutions for the thermal and flow fields, are identical to those studied by Palm, Weber & Kvernvold (1972) in the context of convection in a non-reacting porous medium. In the rotating case, the critical Rayleigh number and corresponding wavenumber depend on $\mathscr{T}$; the effect of rotation is, to order δ^0, to increase R_{0c} and to decrease the horizontal scale of convection cells. In this case, we recover exactly the critical values for the problem of rotating convection in a non-reacting porous layer as considered by Palm & Tyvand (1984) and Vadasz (1998*a*).

The Rayleigh and Taylor numbers are the sole dimensionless parameters controlling convection in the mushy layer. It is instructive to consider the means by which the Rayleigh number was established. A useful insight into this can be obtained from the equation which results from multiplying the perturbation momentum equation by $\hat{\boldsymbol{u}}$ and averaging over the convection cell. This yields

$$0 = \langle K(\delta\bar{\phi}_B + \epsilon\hat{\phi})\hat{\boldsymbol{u}}^2\rangle + R\langle\hat{\theta}\hat{w}\rangle, \tag{3.5}$$

where the angular brackets indicate the appropriate averaging. The first term on the right-hand side of this relation represents the rate of effective viscous dissipation in the porous medium, which is balanced by the rate of release of potential energy. To the leading-order approximation, this relation can be evaluated to become

$$0 = \frac{\pi^4}{4R_{0c}^2}[\mathscr{T}(\sqrt{\mathscr{T}+1}+3)+4(\sqrt{\mathscr{T}+1}+1)] - \frac{\pi^2}{4}(\sqrt{\mathscr{T}+1}+1). \tag{3.6}$$

This relation determines the critical Rayleigh number R_{0c} and is identical to (3.4*a*). Hence, the eigenvalue equation is a statement that a balance between the rate of potential energy release and the rate of effective viscous dissipation in the porous medium is achieved by the fluid element at the onset of linear instability.

The flow field determined by the scalar functions (3.2*c*) and (3.2*d*) corresponds to the well-known case of two-dimensional steady convection in the form of oblique rolls. Owing to the rotation of the system, the local Coriolis acceleration induces a component of the flow which is parallel to the isolines of composition and of local solid fraction in the horizontal planes, i.e. the v_1 component of the flow. For this reason, we refer to the convection as occurring in oblique rolls, the word 'oblique' emphasizing that the streamlines of the flow are confined to the planes oriented at oblique angles to the axes of convection rolls. An account of such convection pattern can be found in Veronis (1959). The leading-order perturbation to the solid fraction (3.2*b*) leads to the formation of vertically oriented channels (in $\bar{x}, \bar{z}$-planes) corresponding to the maximum reduction of the basic-state solid fraction. The horizontal locations of these channels coincide with the positions where the upward flow takes its maximum values and is relatively cold and maximally depleted of solute.

To this point, the derivation of various terms of (3.1) has been relatively straightforward. However, when we consider the coefficients of ϵ^1, we obtain a set of inhomogeneous equations in which the homogeneous terms (proportional to θ_2, ϕ_2, χ_2 or ψ_2) are linearly dependent, because they are identical to those used to obtain the leading-order solutions (3.2). We find that the existence of solutions to these equations requires that

$$R_1 = \alpha R_{1\delta}, \tag{3.7}$$

where

$$R_{1\delta} = \frac{\pi}{4}\frac{(\sqrt{\mathscr{T}+1}+1)(2-\sqrt{\mathscr{T}+1})}{\sqrt{\mathscr{T}+1}}\frac{K_1}{C_S} - \frac{\pi}{2}(\sqrt{\mathscr{T}+1}+1)\frac{St}{C_S}. \tag{3.8}$$

Using this expression, we are now able to determine the solutions at this order. The full expressions are rather complicated and therefore we do not record them here.

We are now in a position to proceed to the next order. We find that the perturbation equations at $O(\epsilon^2)$ are soluble only if

$$R_2 = \alpha^2 R_{2\delta} + R_{2\epsilon}, \tag{3.9}$$

where

$$R_{2\delta} = a(\mathscr{T})\frac{K_2 - K_1}{C_S^2} + b(\mathscr{T})\frac{St}{C_S^2} - c(\mathscr{T})\left(\frac{K_1}{C_S}\right)^2 - d(\mathscr{T})\frac{K_1 St}{C_S^2}$$
$$+ e(\mathscr{T}) + f(\mathscr{T})\left(\frac{St}{C_S}\right)^2 - h(\mathscr{T})\frac{K_1}{C_S}, \tag{3.10a}$$

$$R_{2\epsilon} = -p(\mathscr{T})\frac{K_1}{C_S} - q(\mathscr{T})\left(\frac{K_1}{C_S}\right)^2 + r(\mathscr{T})\frac{K_2}{C_S^2} + s(\mathscr{T}) \tag{3.10b}$$

with

$$p(\mathscr{T}) = \frac{\pi^3}{16}(-\mathscr{T} + 3\sqrt{\mathscr{T}+1} + 1)\frac{\sqrt{\mathscr{T}+1}+1}{\sqrt{\mathscr{T}+1}}, \tag{3.11a}$$

$$q(\mathscr{T}) = \frac{\pi^3}{288}[-16\mathscr{T}^3 - \mathscr{T}^2(97\sqrt{\mathscr{T}+1} - 25) + 3\mathscr{T}(29\sqrt{\mathscr{T}+1} + 83) + 192(\sqrt{\mathscr{T}+1} + 1)]\frac{\sqrt{\mathscr{T}+1}+1}{(\mathscr{T}+1)^{3/2}}, \tag{3.11b}$$

$$r(\mathscr{T}) = \frac{\pi^3}{32}[-\mathscr{T}(7\sqrt{\mathscr{T}+1} - 8) + 22(\sqrt{\mathscr{T}+1} + 1)]\frac{\sqrt{\mathscr{T}+1}+1}{\sqrt{\mathscr{T}+1}}, \tag{3.11c}$$

$$s(\mathscr{T}) = \frac{\pi^3}{16}(\sqrt{\mathscr{T}+1} + 1)^2. \tag{3.11d}$$

Expressions for the functions $a(\mathscr{T})$–$f(\mathscr{T})$ and $h(\mathscr{T})$ appearing in (3.10*a*) are given in the Appendix. Here, we have used the notation in which the functions $a(\mathscr{T})$–$f(\mathscr{T})$, $h(\mathscr{T})$, and $p(\mathscr{T})$–$s(\mathscr{T})$ possess a property that $a(0)$–$f(0)$, $h(0)$, $p(0)$, and $q(0)$–$s(0)$ are positive numbers corresponding to the coefficients *a*–*f*, *g*, *h*, and *k*–*m*, respectively, in the analysis of Amberg & Homsy (1993). The new important results here are the explicit expressions for these particular functions which represent the physical effects associated with the imposed rotation of the system.

The complete expression for the Rayleigh number R then takes the form

$$R = (R_{0c} + \delta R_{1\delta} + \delta^2 R_{2\delta} + \cdots) + \epsilon^2 R_{2\epsilon} + \cdots. \tag{3.12}$$

Clearly, the terms $R_{1\delta}$ and $R_{2\delta}$ represent respectively the $O(\delta)$ and $O(\delta^2)$ corrections to the critical Rayleigh number R_{0c}. Note that this expansion contains no term of $O(\epsilon^1)$. Hence, the sign of $R_{2\epsilon}$ determines whether the bifurcating convection with a two-dimensional oblique-roll pattern is supercritical or subcritical. A more detailed discussion of solvability conditions presented in this section is contained in § 4.

3.2. *Three-dimensional convection with hexagonal symmetry*

In this section, we are concerned with a more general case of three-dimensional convection in the rotating mushy layer. In particular, we identify weakly nonlinear solutions to the system (2.12) which correspond, to the leading order, to steady convecting states with the planform of hexagonal symmetry.

At the leading order of ϵ, $O(\epsilon^0)$, we obtain solutions of the form

$$\theta_1 = -\sin(\pi\bar{z})\eta(\bar{x}, \bar{y}), \tag{3.13a}$$

$$\phi_1 = -\frac{1}{C_S}\frac{\pi^2 + k^2}{\pi}[1 + \cos(\pi\bar{z})]\eta(\bar{x}, \bar{y}), \tag{3.13b}$$

$$\chi_1 = \frac{\pi^2 + k^2}{R_0 k^2}\sin(\pi\bar{z})\eta(\bar{x}, \bar{y}), \tag{3.13c}$$

$$\psi_1 = \sqrt{\mathscr{T}}\frac{\pi(\pi^2 + k^2)}{R_0 k^2}\cos(\pi\bar{z})\eta(\bar{x}, \bar{y}), \tag{3.13d}$$

where the two-dimensional planform which determines the hexagonal symmetry of

these solutions is given by

$$\eta(\bar{x},\bar{y}) = \cos(k\bar{y}) + 2\cos\left(\tfrac{1}{2}\sqrt{3}\,k\bar{x}\right)\cos\left(\tfrac{1}{2}k\bar{y}\right). \tag{3.14}$$

Since there is degeneracy in the linear problem (see the note above), the critical Rayleigh number R_{0c} and corresponding wavenumber k_c are identical to those given by (3.4*a*, *b*) in the case of rolls. Again, we fix R_0 and k at their critical values throughout the further analysis.

The cellular structure of the flow field determined by (3.13*c*) and (3.13*d*) is well known and its detailed analysis can be found elsewhere. We remark here only that the boundaries of the regular hexagonal cells are distorted by the imposed rotation of the system. For a detailed description of this cell distortion as well as a corresponding perspective sketch of the spiral path of a fluid element in such a convection cell the reader is referred to Veronis (1959). The horizontal dependences of the perturbations on the temperature field θ_1 and solid fraction ϕ_1 are of the same form as those of the vertical flow w_1. Therefore, taking into account particular vertical dependences of these perturbations, the isolines in the horizontal planes of both negative (positive) θ_1 and ϕ_1 are qualitatively similar to those of positive (negative) w_1.

The analysis proceeds in the same way as outlined in the preceding section for rolls. We now find that the solvability condition at $O(\epsilon^1)$ implies

$$R_1 = \alpha R_{1\delta} + R_{1\epsilon}, \tag{3.15}$$

where $R_{1\delta}$ has the same form as in the case of rolls (see equation (3.8)) and

$$R_{1\epsilon} = \frac{\pi^2}{4}\frac{(\mathscr{T} - 2\sqrt{\mathscr{T}+1} - 1)(\sqrt{\mathscr{T}+1}+1)}{\sqrt{\mathscr{T}+1}}\frac{K_1}{C_S}. \tag{3.16}$$

Thus, we find that the complete expansion for the Rayleigh number can be expressed as

$$R = (R_{0c} + \delta R_{1\delta} + \cdots) + \epsilon R_{1\epsilon} + \cdots, \tag{3.17}$$

so that the bifurcation to the three-dimensional convection with hexagonal symmetry is, in general, transcritical. The important result here is that $R_{1\epsilon}$ can be positive, negative or zero. This suggests that the hexagonal convection with upflow at the centres can be either subcritically or supercritically bifurcating, depending on the strength of the imposed rotational constraint. Note that the sign change in $R_{1\epsilon}$ was not possible in the non-rotating problem studied by Amberg & Homsy (1993); $R_{1\epsilon}$ was always negative and so the bifurcation to regular hexagons with upflow at the centres was subcritical in any case. The parameter regime where these particular results apply is determined in the next section.

4. Discussion

The solvability conditions (3.7) and (3.9) for the two-dimensional oblique-roll solution, and (3.15) for the hexagonal solution reveal a number of interesting and important results regarding the nature of the onset of instability to infinitesimal steady convection as well as the onset of finite-amplitude steady motions in the rotating mushy layer. These results are discussed in detail below.

There are some possibilities for checking the results of our analysis. For $\mathscr{T} = 0$, the case of a non-rotating mushy layer has to be recovered, which for the two-dimensional roll and hexagonal patterns was reported by Amberg & Homsy (1993). In the rotating

case, $\mathscr{T} > 0$, there are two previous studies which are appropriate for testing our results. First, Vadasz (1998*a*) performed both linear and weakly nonlinear stability analyses of two-dimensional rotating convection in a passive porous medium with uniform permeability; our system corresponds to this problem in the limit $\delta \to 0$. Second, in the case of setting $\epsilon = 0$, the problem of linear stability in the rotating mushy layer has to be recovered; this was recently studied by Guba & Bod'a (1998).

4.1. *Two-dimensional convection in the form of oblique rolls*

4.1.1. *Linear stability results*

To discuss the properties of the roll solutions presented in § 3.1, we focus first on the case of setting $\epsilon = 0$ in these solutions. This particular case recovers the results of the linearized theory.

For $\mathscr{T} = 0$, the leading-order, first and second correction terms to the linear Rayleigh number reduce to

$$R_{0c} = 2\pi, \tag{4.1a}$$

$$R_{1\delta} = \frac{\pi}{2}\frac{K_1}{C_S} - \pi\frac{St}{C_S}, \tag{4.1b}$$

$$R_{2\delta} = \left(\frac{\pi}{24} - \frac{1}{16\pi}\right) - \left(\frac{\pi}{12} - \frac{3}{8\pi}\right)\frac{K_1}{C_S} + \frac{\pi}{3}\frac{K_2 - K_1}{C_S^2} - \left(\frac{5\pi}{48} + \frac{1}{16\pi}\right)\left(\frac{K_1}{C_S}\right)^2 + \left(\frac{\pi}{2} + \frac{4}{\pi}\right)\frac{St}{C_S^2} + \frac{3\pi}{4}\left(\frac{St}{C_S}\right)^2 - \frac{\pi}{4}\frac{K_1 St}{C_S^2}. \tag{4.1c}$$

These results should be in an agreement with the linear stability results for the non-rotating problem in Amberg & Homsy (1993) (see their equations (3.3*d*), (3.4) and (3.5*b*)). However, note that the numerical values of coefficients a, c and g in the expression for $R_{2\delta}$ were incorrectly given as $a \approx 0.728\,888$, $c \approx 0.232\,244$ and $g \approx 0.356\,825$ in table 1 of their paper. These should equal to $a \approx 1.047\,198$, $c \approx 0.347\,144$ and $g \approx 0.142\,433$, as revealed by the values of the corresponding functions $a(\mathscr{T})$, $c(\mathscr{T})$ and $h(\mathscr{T})$ at $\mathscr{T} = 0$ in the present analysis (G. Amberg, private communication, 1997).

For a later comparison with the linear stability results for the rotating problem, it is worth noting some properties of the results given by equations (4.1). It is clear from (4.1*a*) that the leading-order, $O(\delta^0)$, value of the linear Rayleigh number for the onset of infinitesimal steady convection is constant. From equation (4.1*b*) it follows that the linear Rayleigh number, correct to $O(\delta^1)$, decreases linearly as the Stefan number St increases so that the system becomes more unstable as St increases. Further, the variation in the linear Rayleigh number with the linear measure of the permeability variations K_1 is characterized by stabilizing the system when K_1 increases. Note also that increasing K_1 has the effect of decreasing the permeability of the mushy layer. The effect of variations in the compositional ratio C_S, or, turning back to the original unscaled variable, in $\mathscr{C}$ ($\mathscr{C} = C_S/\delta$), on the linear Rayleigh number is determined by the strength of K_1 relative to St according to (4.1*b*); when $K_1 > 2St$, we see that increasing $\mathscr{C}$ represents a destabilizing effect whereas it tends to stabilize the system when $K_1 < 2St$.

When the rotational constraint is present in the system ($\mathscr{T} > 0$) and still supposing that $\epsilon = 0$, we obtain, in fact, the solutions to the linear stability problem in the rotating mushy layer. An analysis of such a problem using the same physical model

of the mushy layer as the model considered here was recently carried out by Guba & Bod'a (1998). Although they adopted a different scaling for the Stefan number, namely (in their notation) $S = \bar{S}/\delta$ where $\bar{S} = O(1)$ as $\delta \to 0$ (see also Anderson & Worster 1995), it is possible to compare their results with the results of the present study. In order to make this comparison, we reconsider their results for the leading-order and first correction terms to the linear critical Rayleigh number of steady mode of instability (see the real part of their equation (3.6)) in which we take $k = \pi(\mathscr{T}+1)^{1/4}$, $\bar{S} = \delta St$, $\Omega \equiv 1 + \bar{S}/C_S = 1 + \delta St/C_S$ and find that

$$R = \pi(\sqrt{\mathscr{T}+1}+1) + \delta\left[\frac{\pi}{4}\frac{(\sqrt{\mathscr{T}+1}+1)(2-\sqrt{\mathscr{T}+1})}{\sqrt{\mathscr{T}+1}}\frac{K_1}{C_S} - \frac{\pi}{2}(\sqrt{\mathscr{T}+1}+1)\frac{St}{C_S}\right]$$
$$+\delta^2\left[\left(\frac{\pi}{4}+\frac{2}{\pi}\right)(\sqrt{\mathscr{T}+1}+1)\frac{St}{C_S^2} + \frac{3\pi}{8}(\sqrt{\mathscr{T}+1}+1)\left(\frac{St}{C_S}\right)^2\right.$$
$$\left.+\frac{\pi}{8}\frac{(\sqrt{\mathscr{T}+1}+1)(\sqrt{\mathscr{T}+1}-2)}{\sqrt{\mathscr{T}+1}}\frac{K_1 St}{C_S^2}\right] + O(\delta^2). \tag{4.2}$$

We see that this expression is correct to $O(\delta)$ and is in agreement with the results of the present analysis (see equations (3.4*a*) and (3.8) above). The $O(\delta^2)$ terms that appear in this expression should be compared with the particular terms contained in (3.10*a*) of the present analysis. Note that it is not possible to recover all of the $O(\delta^2)$ contributions since the linear stability analysis by Guba & Bod'a (1998) was performed to obtain the results correct to $O(\delta^1)$ only.

Even though the formal solution to the linear stability problem in the rotating mushy-layer system was given in our earlier paper, we still need simple physical arguments to explain the results appearing at particular orders of δ. An attempt to present such arguments is given below.

In contrast to the non-rotating problem, the leading-order, $O(\delta^0)$, value of the Rayleigh number for the onset of infinitesimal convection in the rotating mushy layer is no longer constant but depends on the value of the Taylor number $\mathscr{T}$. As expected, the leading-order effect of $\mathscr{T}$ is to increase R_{0c} and therefore to stabilize the system, as can be deduced from equation (3.4*a*). The physical explanation for this can be found, for example, in the equation for a stream function of the flow in the $(\bar{x}, \bar{z})$-plane, $\partial\chi_1/\partial\bar{x}$. Specifically, taking the $\bar{y}$-component of the curl of the perturbation momentum equation, we find that at $O(\epsilon^0)$

$$\nabla^2\frac{\partial\chi_1}{\partial\bar{x}} = R_0\frac{\partial\theta_1}{\partial\bar{x}} + \sqrt{\mathscr{T}}\frac{\partial v_1}{\partial\bar{z}}. \tag{4.3}$$

The rotation of the system introduces the Coriolis force and a 'solutal wind' component is generated. The solutal wind field is an analogue of the thermal wind field which is a familiar concept in geophysical problems. Here, it describes a balance between a horizontal gradient of the concentration field and a vertical shear of the flow field component v_1 (the so-called zonal velocity) normal to the gradient of the concentration field. In equation (4.3), this balance is given by the terms appearing on the right-hand side. Obviously, the balance is not complete because a third term, the viscous dissipation in the porous medium, is also present. However, the inhibition of convection is, to the order shown, clearly traceable to the solutal wind because a good part of the force which releases potential energy is balanced by the rotational constraint which is energetically inactive. The larger the rotation rate, the larger the

zonal velocity. Hence, less potential energy is released for a given horizontal gradient of the concentration field. Such behaviour is analogous to the linear aspects of the stability problem studied in relation to a steady Boussinesq Bénard convection in a rotating fluid layer (see e.g. Chandrasekhar 1961).

The asymptotic nature of the present model is such that it allows the physical effects inherent in the mushy layer to be incorporated in the analysis as perturbations to the near-eutectic approximation of the system. These physical effects include the interaction between flow field and temperature (or, equivalently, composition) due to the dependence of permeability on the local solid fraction, and the interaction of temperature and local solid fraction due to the local release of latent heat and solvent as the local freezing occurs. Even in the linear regime the nature of these physical effects can be, as we shall see, crucially altered by the inclusion of additional physical effects associated with the imposed rotational constraint. This is indicated by the fact that some of the functions of $\mathscr{T}$ appearing in (3.8) and (3.10*a*) can change sign, and therefore reversals in the dependences of the linear Rayleigh number on the corresponding system control parameters can become possible.

For the remainder of the discussion of linear stability results, we restrict ourselves to discuss only the first-order correction term $R_{1\delta}$ given by (3.8). In discussing the effect of variations in the Stefan number St on the linear Rayleigh number, one might expect that the destabilizing effect associated with increasing St, which is known to be the case in the non-rotating problem, will be suppressed by the presence of rotation, owing to its general constraining effect upon the convection. However, according to (3.8), the Stefan number St appears in combination with the function of the Taylor number $\mathscr{T}$ which is both positive and monotonically increasing as $\mathscr{T}$ increases. For a positive value of $\mathscr{T}$, this implies that the linear Rayleigh number decreases more rapidly with increasing Stefan number St than it would in the non-rotating system. In other words, the effect of $\mathscr{T}$ is to amplify the physical effect of varying St.

A more dramatic effect of the presence of rotational constraint in the system appears in connection with the effect upon the linear Rayleigh number of varying the permeability coefficient K_1. In particular, we find that the stabilizing effect of increasing K_1 is now constrained to the range $0 \leqslant \mathscr{T} < 3$ of Taylor numbers. When $\mathscr{T} > 3$, increasing K_1, perhaps surprisingly, can no longer stabilize the system. The following physical argument might, perhaps, provide some insight into this behaviour. The term proportional to K_1/C_S in the expression (3.8) is associated with the non-uniformity in permeability due to the $O(\delta^1)$ correction to the basic-state solid fraction, $\bar{\phi}_{B0}$. To be more specific, the terms by which K_1/C_S enters the solvability condition in the first order are given by

$$-\alpha K_1 \bar{\phi}_{B0} \nabla^2 \frac{\partial \chi_1}{\partial \bar{x}} \quad \text{and} \quad -\alpha K_1 \sqrt{\mathscr{T}}\, \bar{\phi}_{B0} \frac{\partial v_1}{\partial \bar{z}}, \tag{4.4}$$

which partly force a stream function correction $\partial \chi_2/\partial \bar{x}$ at $O(\epsilon^1)$. The first of these terms is associated with the $\bar{y}$-component of the local vorticity arising from the Darcy friction at $O(\epsilon^0)$; this term is present even if the system is not rotated. The second term is associated with the solutal wind field generated by the rotation of the system at $O(\epsilon^0)$; clearly, this term has no counterpart in the non-rotating problem. Examining these two terms, we find that the effect of the term proportional to the solutal wind field is to offset the constraining term proportional to the $\bar{y}$-component of the local vorticity. It is for this reason that, for a sufficiently large value of $\mathscr{T}$, the system can become more unstable as K_1 increases.

A further important effect of the presence of rotational constraint is a possibility to

alter qualitatively the dependence of the linear Rayleigh number on the compositional ratio C_S. From (3.8) it can readily be seen that the effect of variations in C_S depends on the relative strength of $(2-\sqrt{\mathscr{T}+1})K_1$ and $2\sqrt{\mathscr{T}+1}St$. More specifically, we find that when $K_1 > 2St$ and $\mathscr{T} < -1 + 4K_1^2/(K_1+2St)^2$, increasing C_S leads to a decrease in the linear Rayleigh number and therefore is destabilizing. This behaviour is qualitatively similar to that in the non-rotating case when $K_1 > 2St$. However, once $\mathscr{T} > -1+4K_1^2/(K_1+2St)^2$, keeping $K_1 > 2St$, the effect of increasing C_S is stabilizing. Finally, if K_1 is decreased through $2St$, the result identified in the non-rotating case qualitatively holds true.

4.1.2. *Weakly nonlinear solutions*

We consider further the case where ϵ is non-zero. Note that ϵ has been introduced as the perturbation parameter defined by (3.1*e*) and represents the small but finite amplitude of the perturbation variables according to (2.9*c*)–(2.9*f*).

When the Taylor number $\mathscr{T}$ is set equal to zero, we can find from (3.10*b*) and (3.11) that the finite-amplitude correction term $R_{2\epsilon}$ takes the value

$$R_{2\epsilon} = \frac{\pi^3}{4} - \frac{\pi^3}{2}\frac{K_1}{C_S} - \frac{8\pi^3}{3}\left(\frac{K_1}{C_S}\right)^2 + \frac{11\pi^3}{4}\frac{K_2}{C_S^2}. \tag{4.5}$$

This expression agrees with the results of Amberg & Homsy (1993) (see their equation (3.5*c*) with constants h, k, l and m given numerically in table 1 of their paper). In order for a later comparison with our result for $R_{2\epsilon}$ in the rotating system to be clearer, it is helpful to review the basic properties of (4.5) as discussed by Amberg & Homsy. When $K_1 = K_2 = 0$, the expression (4.5) becomes $R_{2\epsilon} = \pi^3/4$ so that the bifurcation is always supercritical. This situation corresponds to the finite-amplitude convection in a passive porous medium with constant permeability studied by Palm *et al.* (1972). When the permeability variations with the local solid fraction are taken into account, the subcritical bifurcation to convection in the form of two-dimensional simple rolls may occur. In particular, when K_1 is assumed to be non-zero and K_2 is, for simplicity, set equal to zero, a critical value of the parameter combination K_1/C_S can be identified, namely $K_1/C_S \approx 0.226$, above which the bifurcation is subcritical and below which the bifurcation is supercritical. For a positive value of K_2, which is appropriate for a permeability function of the kind proposed by Worster (1992), the last term in (4.5) is positive. Therefore, for fixed values of K_1 and C_S, the increasing K_2 has the effect of increasing the tendency towards the supercritical bifurcation to rolls.

In the rotating case, $\mathscr{T} > 0$, substituting $K_1 = K_2 = 0$ in (3.10*b*) yields

$$R_{2\epsilon} = \frac{\pi^3}{16}(\sqrt{\mathscr{T}+1}+1)^2, \tag{4.6}$$

which indicates the supercriticality of the bifurcation, regardless of the value of $\mathscr{T}$. This agrees with the results of weakly nonlinear analysis for the rotating convection in a passive porous layer by Vadasz (1998*a*).

Not restricted by considering particular values of the control parameters, the results represented by equations (3.10*b*) and (3.11) correspond to the onset of finite-amplitude convection in the rotating mushy layer. Nevertheless, the case of particular simplicity which throws some light on the mechanism by which the rotation controls the subcritical bifurcation to oblique rolls can be obtained by keeping $K_2 = 0$ in (3.10*b*). In this case, $R_{2\epsilon}$ depends on both the simple parameter combination K_1/C_S and Taylor number $\mathscr{T}$ only. A boundary marking the transition from subcritical

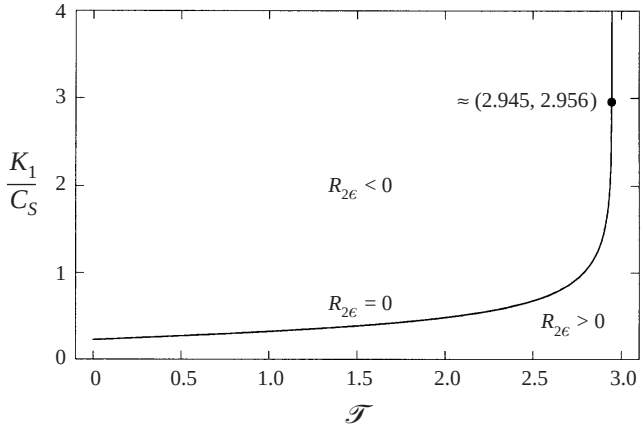

FIGURE 2. Transition boundary from subcritical to supercritical oblique rolls as a function of the Taylor number $\mathscr{T}$ and the parameter combination K_1/C_S for fixed $K_2 = 0$. The solid curve separates the regions where the subcritical ($R_{2\epsilon} < 0$) and supercritical ($R_{2\epsilon} > 0$) oblique rolls are predicted. Within the range $0 \leqslant \mathscr{T} < \mathscr{T}_U$, where the upper bound $\mathscr{T}_U$ is calculated numerically to give 2.945..., the solid curve corresponds to the analytical expression (4.7). Once $\mathscr{T}$ attains the value $\mathscr{T}_U$, the transition boundary continues to be represented by the vertical solid line starting at the point $(\mathscr{T}_U, (K_1/C_S)_U) \approx (2.945, 2.956)$.

to supercritical oblique rolls in the parameter space $(\mathscr{T}, K_1/C_S)$ is shown in figure 2. This boundary is determined by the condition for vertical bifurcation, i.e. $R_{2\epsilon} = 0$. If $0 \leqslant \mathscr{T} < \mathscr{T}_U$, where the upper bound $\mathscr{T}_U$ on $\mathscr{T}$ may be readily computed to give 2.945..., we find that this boundary is given by the following explicit analytical formula:

$$\frac{K_1}{C_S} = 3[-12(\sqrt{\mathscr{T}+1}+1) - 9\mathscr{T}(\sqrt{\mathscr{T}+1}+2) + 3\mathscr{T}^2(\sqrt{\mathscr{T}+1}-2) + \sqrt{D}]$$
$$\times[384(\sqrt{\mathscr{T}+1}+1) + 48\mathscr{T}(7\sqrt{\mathscr{T}+1}+11)$$
$$-3\mathscr{T}^2(24\sqrt{\mathscr{T}+1}-5) - \mathscr{T}^3(16\sqrt{\mathscr{T}+1}+113)]^{-1}, \tag{4.7}$$

where

$$D = 3360(\sqrt{\mathscr{T}+1}+1) + 120\mathscr{T}(79\sqrt{\mathscr{T}+1}+93) + \mathscr{T}^2(8328\sqrt{\mathscr{T}+1}+12657)$$
$$+3\mathscr{T}^3(466\sqrt{\mathscr{T}+1}+1541) - \mathscr{T}^4(11000\sqrt{\mathscr{T}+1}+917)$$
$$-5\mathscr{T}^5(58\sqrt{\mathscr{T}+1}+143) - 32\mathscr{T}^6. \tag{4.8}$$

Once the value $\mathscr{T}_U$ is reached, the transition boundary is found to be invariant as the parameter combination K_1/C_S changes so that it continues as the vertical line starting at a point $(\mathscr{T}_U, (K_1/C_S)_U) \approx (2.945, 2.956)$. This upper part of the transition boundary is also shown in figure 2. Note that when $\mathscr{T} = 0$, the critical value of K_1/C_S becomes $(\sqrt{105}-3)/32 \approx 0.226$ which corresponds to the critical value obtained from the non-rotating theory.

In interpreting the result displayed in figure 2, we first note that the possibility of finite-amplitude convecting states in the rotating mushy layer is brought about by the same particular physical effect which gave rise to the finite-amplitude motions in the non-rotating system studied by Amberg & Homsy (1993). In fact, they are both due to the term proportional to K_1/C_S, namely the nonlinear variations of permeability

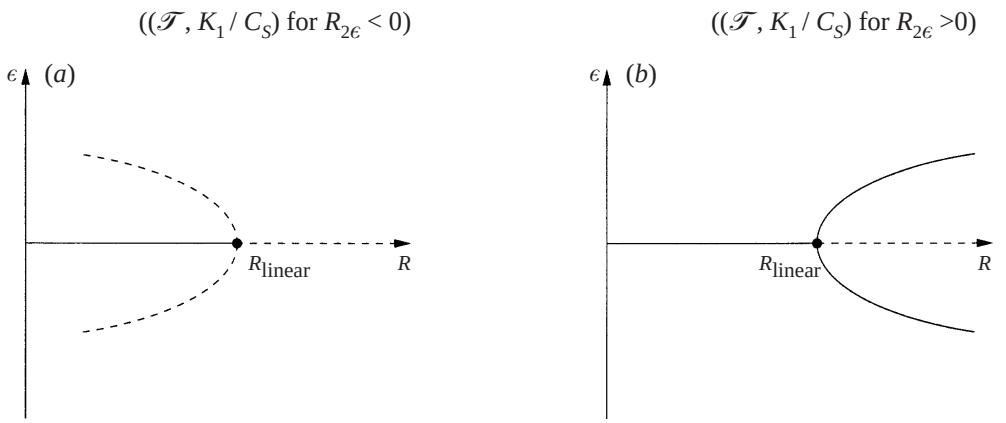

FIGURE 3. Bifurcation diagram for two-dimensional oblique rolls. The amplitude of the weakly nonlinear perturbations, ϵ, is plotted *vs.* Rayleigh number, R, for two cases. The value R_{linear} corresponds to the linear critical Rayleigh number given by $R_{\text{linear}} = R_{0c} + \delta R_{1\delta} + O(\delta^2)$. Solid and dashed curves represent the presumed stable and unstable portions of the solution branches, respectively ('presumed' since an issue of stability is not explicitly pursued here). (*a*) The parameter pair $(\mathscr{T}, K_1/C_S)$ corresponds to initially subcritically bifurcating oblique rolls with $K_2 = 0$, and (*b*) $(\mathscr{T}, K_1/C_S)$ corresponds to initially supercritically bifurcating oblique rolls with $K_2 = 0$ (cf. figure 2).

with the leading-order perturbation to the basic-state solid fraction. In the rotating system, in addition, there is an important physical effect which effectively controls the presence of the subcritical bifurcation, as indicated by figure 2. This stabilizing effect of rotation at finite amplitudes is caused by the Coriolis force which counteracts the destabilizing effect associated with the nonlinear permeability variations. This phenomenon is, in a sense, opposite to the alignment process suggested by Veronis (1959) in the context of steady rotating Boussinesq Bénard convection, in which the Coriolis force counteracts the stabilizing effect of the nonlinear momentum advection term.

Figure 3 shows a schematic bifurcation diagram for two-dimensional oblique rolls. In this figure, the amplitude of the weakly nonlinear solutions, ϵ, is plotted *vs.* Rayleigh number, R. The diagram is shown for two cases of the parameter pair $(\mathscr{T}, K_1/C_S)$, corresponding to initially subcritically (figure 3*a*) and supercritically (figure 3*b*) bifurcating oblique rolls with $K_2 = 0$ (cf. figure 2).

The term proportional to K_2 in the expression (3.10*b*) is associated with the second-order non-uniformity in permeability due to the basic-state solid fraction and its perturbations. For $\mathscr{T} = (323 + 15\sqrt{617})/98 \approx 7.098$, this term is zero and therefore the nature of the bifurcation is quite insensitive to the quadratic measure of permeability variations. For values of $\mathscr{T}$ smaller (larger) than this value the term involving K_2 is positive (negative), thus increasing the tendency towards supercritical (subcritical) bifurcation. An interesting result that emerges from this is that oblique rolls can be subcritically bifurcating in the rotating system even when the linear permeability variations with the perturbation to the solid fraction are excluded.

Based on Darcy's equation to model the fluid flow, the present model of the mushy layer ceases to be valid when it predicts negative solid fraction. Following Amberg & Homsy (1993), we equate the basic-state solid fraction with its perturbation (3.2*b*) and identify the perturbation amplitude

$$\epsilon_{\max}(\mathscr{T}) = \frac{\delta}{2\pi(\sqrt{\mathscr{T}+1}+1)} + O(\delta^2), \tag{4.9}$$

which, for a given value of δ, gives us the maximum allowed value of ϵ for the validity of the model. It is important to note that the particular form of $\epsilon_{\max}$ depends on the normalization condition imposed in the linear stability problem. In the present analysis, we have used the normalization in which the maximum value of the eigenfunction representing perturbation to the thermal field is equal to unity.

4.1.3. *Structure of the weakly nonlinear solutions*

In this section, we examine the effect of rotation on the structure of finite-amplitude two-dimensional solutions. This effect can be appropriately appreciated in terms of the vertical and horizontal averages of perturbation fields,

$$\langle f(\bar{x},\bar{z})\rangle_{\bar{z}} = \int_0^1 f(\bar{x},\bar{z})\,\mathrm{d}\bar{z}, \tag{4.10a}$$

$$\langle f(\bar{x},\bar{z})\rangle_{\bar{x}} = \frac{2}{\lambda_c}\int_0^{\lambda_c/2} f(\bar{x},\bar{z})\,\mathrm{d}\bar{x}, \tag{4.10b}$$

respectively, where $f(\bar{x},\bar{z})$ denotes a particular perturbation quantity and λ_c is the wavelength of the perturbation. The corresponding results presented below provide useful information about the way in which the rotation manifests itself in the flow.

In all the calculations, we use the illustrative set of parameter values $St = 1$, $C_S = 1$, $K_2 = 0$ and $\delta = 0.3$. We set the linear measure of permeability variations $K_1 = 3$ and consider the values of $\mathscr{T}$ below $\mathscr{T}_U \approx 2.945$. Accordingly, the results presented correspond to subcritically bifurcating convecting states (see figure 2). We take the perturbation amplitude $\epsilon = 0.0155$ throughout, this being close to the critical value for breakdown of the model when $\mathscr{T} = 2.9$, $\epsilon_{\max}(2.9) \approx 0.016$.

The vertically averaged perturbation quantities are plotted as functions of the horizontal coordinate $\bar{x}$ in figure 4 for different values of $\mathscr{T}$. Each graph has been displayed in a convection cell corresponding to the interval $0 \leqslant \bar{x} \leqslant \lambda_c(\mathscr{T})/2$. Notice that graphs in (*a*), (*b*) and (*d*) are symmetric, while graphs in (*c*) are antisymmetric with respect to the line $\bar{x} = 0$. Figure 4(*a*), which shows the plots for the vertically averaged perturbation to the solid fraction, $\langle \epsilon\hat{\phi}\rangle_{\bar{z}}$, should be compared with figure 4(*b*), which shows the profiles for the vertical flow averaged over the depth of the layer, $\langle w\rangle_{\bar{z}}$. Note that positive solid-fraction perturbations show where the solidification is enhanced, while the negative perturbations correspond to the local melting of the dendrites. For a fixed value of $\mathscr{T}$, we see that there is a localization of the upflow into the relatively narrow region in the vicinity of $\bar{x} = 0$, where the corresponding solid-fraction perturbation leads to a substantial reduction in the basic-state solid fraction. Note also that for the non-rotating case, the minimum value of the solid fraction is almost zero, suggesting the formation of a chimney; for the parameter values used, this minimum is attained at a certain vertical level within the mushy layer. The notable feature of the plots shown in figure 4(*a*) is the behaviour as the Taylor number varies: as $\mathscr{T}$ is increased, the magnitude of $\langle \epsilon\hat{\phi}\rangle_{\bar{z}}$ decreases. This is indicative of a tendency to suppress the formation of the chimney in the region of upflow in the rotating mushy layer. The explanation for this is that the rotational constraint tends to counter a positive nonlinear feedback, which is known to be responsible for the formation of chimneys in the non-rotating system (e.g. Worster 1992; Tait & Jaupart 1992); as $\mathscr{T}$ increases, a fluid parcel displaced upwards becomes more and more confined to a plane transverse to the angular velocity vector, and therefore it becomes surrounded by both chemically and thermally more and more similar surroundings. As a result, with the relatively large thermal diffusivity compared to the

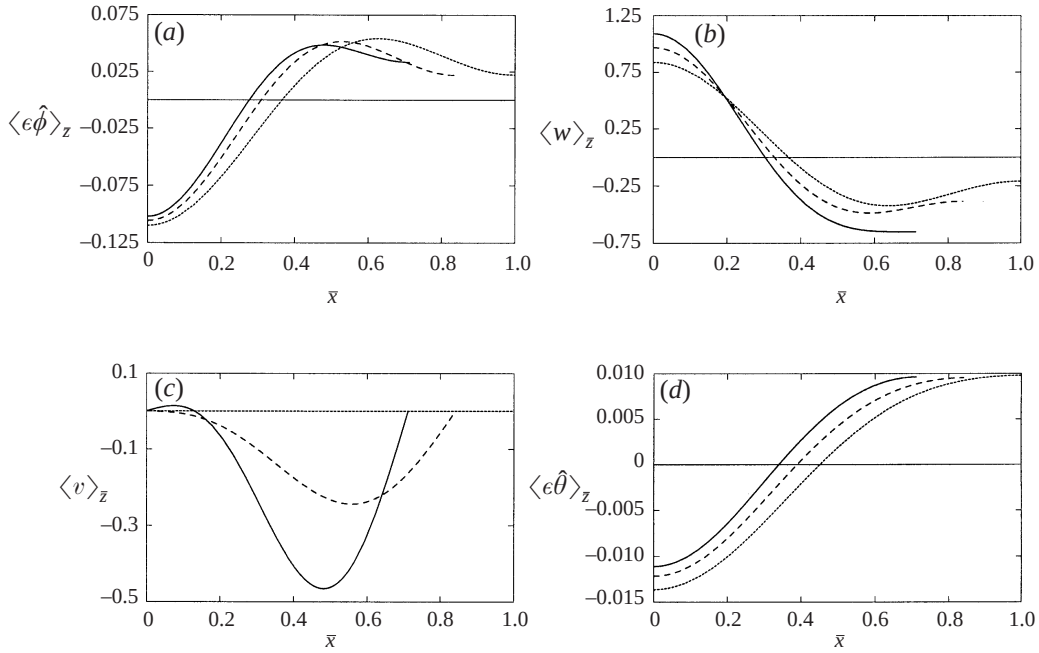

FIGURE 4. The vertically averaged perturbation quantities as functions of the horizontal coordinate $\bar{x}$ for different values of the Taylor number $\mathscr{T}$. In each case $St = 1$, $C_S = 1$, $K_1 = 3$, $K_2 = 0$, $\delta = 0.3$ and $\epsilon = 0.0155$. The short-dashed, long-dashed, and solid lines correspond to the values $\mathscr{T} = 0$, 1 and 2.9, respectively. The parameter values used correspond to subcritically bifurcating convecting states. Each graph has been plotted in a convection cell corresponding to the interval $0 \leqslant \bar{x} \leqslant \lambda_c(\mathscr{T})/2$, where $\lambda_c(\mathscr{T}) = 2\pi/k_c(\mathscr{T})$. (*a*) $\langle \epsilon\hat{\phi} \rangle_{\bar{z}}$ *vs.* $\bar{x}$, (*b*) $\langle w \rangle_{\bar{z}}$ *vs.* $\bar{x}$, (*c*) $\langle v \rangle_{\bar{z}}$ *vs.* $\bar{x}$, (*d*) $\langle \epsilon\hat{\theta} \rangle_{\bar{z}}$ *vs.* $\bar{x}$. Notice that graphs in (*a*), (*b*) and (*d*) are symmetric, while graphs in (*c*) are antisymmetric with respect to the line $\bar{x} = 0$.

solute diffusivity, the parcel does not need to adapt to its new chemical surroundings by as much dissolution of surrounding crystals for the same perturbation as it does in the non-rotating system. Notice, from the plots in figure 4(*b*), that as $\mathscr{T}$ increases, the amplitude of $\langle w \rangle_{\bar{z}}$ in this dynamic regime increases. The corresponding change in the magnitude of vertically averaged zonal flow, $\langle v \rangle_{\bar{z}}$, is, however, much greater (see figure 4*c*). The flow therefore becomes dominated by rotation.

Figure 4(*c*) shows the profiles for the vertically averaged zonal velocity, $\langle v \rangle_{\bar{z}}$. We first note that the zonal flow does not appear in the non-rotating case, so that $\langle v \rangle_{\bar{z}}$ is zero when $\mathscr{T} = 0$. Also note that $\langle v \rangle_{\bar{z}}$ vanishes at the marginal stability limit; that is, the part v_1 of v which contributes to the solutal wind makes no contribution to $\langle v \rangle_{\bar{z}}$. Therefore, the quantity $\langle v \rangle_{\bar{z}}$ represents essentially a measure of a part of zonal flow which is produced by the nonlinear interaction between the local solid fraction, and hence the permeability, and convection. The characteristic property common to both profiles shown in figure 4(*c*) is a relatively strong asymmetry, with the field concentrated within the right, rather than the left half-cell. This asymmetry is perhaps more pronounced as $\mathscr{T}$ increases. Notice also that the zonal flow is predominantly negative throughout each of the cells corresponding to different values of $\mathscr{T}$.

Finally, in figure 4(*d*), we show the plots for the perturbation to the thermal field averaged over the depth of the layer, $\langle \epsilon\hat{\theta} \rangle_{\bar{z}}$. For a fixed value of $\mathscr{T}$, by comparing the plots in figure 4(*d*) with the corresponding plots in figure 4(*b*), it can be clearly

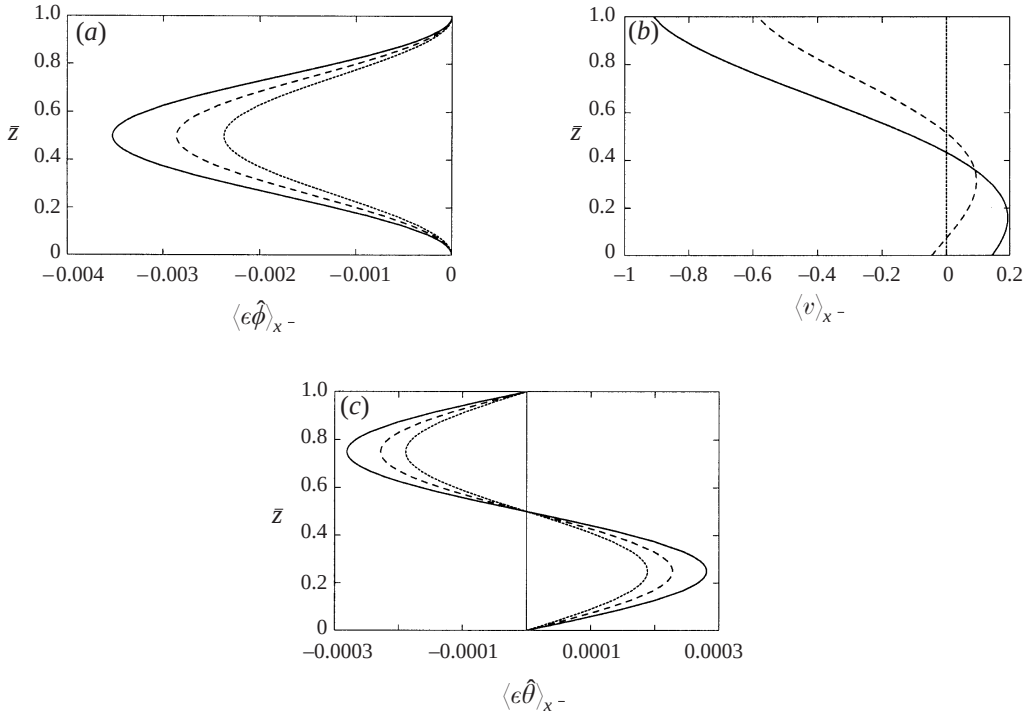

FIGURE 5. The horizontally averaged perturbation quantities as functions of height $\bar{z}$ for different values of the Taylor number $\mathscr{T}$. The parameter values are the same as for figure 4. (*a*) $\langle \epsilon\hat{\phi} \rangle_{\bar{x}}$ *vs.* $\bar{z}$, (*b*) $\langle v \rangle_{\bar{x}}$ *vs.* $\bar{z}$, (*c*) $\langle \epsilon\hat{\theta} \rangle_{\bar{x}}$ *vs.* $\bar{z}$.

seen that the rising fluid is relatively cold and depleted of solute. Notice also that the thermal-field perturbations are considerably smaller in amplitude than the other disturbances for the same value of $\mathscr{T}$. The increase in $\mathscr{T}$ has the effect of decreasing the magnitude of the cold anomaly (solute depleted) within the left half-cell; the warm anomaly (solute rich) within the right half-cell remains almost unaltered. This asymmetric pattern of behaviour is akin to that in figure 4(*c*) and results because as $\mathscr{T}$ increases, the strength of nonlinearly generated zonal flow increases, which allows an advection of more solute along the axis of convection roll.

The horizontal averages of perturbation fields as functions of height $\bar{z}$ are displayed in figure 5 for the same set of values of $\mathscr{T}$ as in figure 4. For a given value of $\mathscr{T}$, the solid fraction perturbation, $\langle \epsilon\hat{\phi} \rangle_{\bar{x}}$, exhibits purely sinusoidal variation, with negative values throughout the depth and the peak at the mid-depth of the layer (figure 5*a*). Recall that in the absence of convection the leading-order solid-fraction distribution is linear in $\bar{z}$. Hence, $\langle \epsilon\hat{\phi} \rangle_{\bar{x}}$ reflects the distortion of the mean solid fraction profile caused by nonlinear processes. Although the magnitude of the perturbation increases with $\mathscr{T}$, close inspection of the numerical results shows that the change in amplitude of $\langle \epsilon\hat{\phi} \rangle_{\bar{x}}$ corresponding to $\mathscr{T} = 0$ and 2.9 is less than about 10% of that for $\langle \epsilon\hat{\phi} \rangle_{\bar{z}}$ (see figure 4*a*). Correspondingly, the dynamical effect of convection, influenced by rotation, to inhibit the dissolution of dendrites in the regions of upflow is much stronger than to enhance the dissolution in the mid-depth region of the mushy layer.

In the nonlinear regime, the form of the vertical flow is such that $\langle w \rangle_{\bar{x}} = 0$; this feature of the flow is also independent of the rotation of the system.

Similarly as in the case of solid fraction, in the conductive state, the temperature

distribution varies, to the leading order, linearly with $\bar{z}$. Thus, $\langle \epsilon\hat{\theta}\rangle_{\bar{x}}$ shown in figure 5(*c*) measures the nonlinear effects on the mean temperature field. The variations are purely sinusoidal and reflect the upward convection of relatively cold fluid, and downward convection of relatively warm fluid. As $\mathscr{T}$ is increased, both anomalies grow in amplitude; this effect is localized approximately in the regions where the zonal flow is enhanced (see figure 5*b*). The change in the amplitude of $\langle \epsilon\hat{\theta}\rangle_{\bar{x}}$ corresponding to $\mathscr{T} = 0$ and 2.9 is, however, only about 3% of that for $\langle \epsilon\hat{\theta}\rangle_{\bar{z}}$ (see figure 4*d*). The horizontally averaged thermal field therefore differs only slightly from its non-rotating counterpart.

4.2. *Three-dimensional convection with hexagonal symmetry*

We now turn our attention to discussing three-dimensional hexagonal solutions presented in § 3.2.

4.2.1. *Linear stability results*

First, we set the perturbation amplitude $\epsilon = 0$, which recovers the linear stability results. The Rayleigh number for the linear stability is, correct to $O(\delta^1)$, identical to that for rolls, and therefore it does not need a separate discussion; the reader is referred to the previous subsection where the discussion of its properties can be found.

4.2.2. *Weakly nonlinear solutions*

We next consider the case where the perturbation amplitude ϵ is non-zero. Since the first finite-amplitude correction term in the expression (3.17) is linearly dependent on ϵ, in contrast to the quadratic proportionality in the case of rolls, the bifurcation to the hexagonal convection is, in general, transcritical.

By setting $\mathscr{T} = 0$, the expression (3.16) becomes

$$R_{1\epsilon} = -\frac{3\pi^2}{2}\frac{K_1}{C_S}, \tag{4.11}$$

which corresponds to that in the analysis of hexagons in Amberg & Homsy (1993). Note that the sense of the flow is determined by the sign of the perturbation amplitude ϵ; upflow at the centres of regular hexagons corresponds to $\epsilon > 0$ and downflow to $\epsilon < 0$. Since both K_1 and C_S are always positive, the nature of the transcritical bifurcation to regular hexagons cannot change in the non-rotating system. That is, more specifically, the bifurcation to hexagons with upflow at the centres is always subcritical (Amberg & Homsy 1993; but cf. Anderson & Worster 1995).

In the rotating system ($\mathscr{T} > 0$), the nature of the transcritical bifurcation to convection with hexagonal symmetry can vary, depending crucially on the value of the Taylor number $\mathscr{T}$. This is clearly suggested by the fact that a particular function of $\mathscr{T}$ appearing in association with the parameter combination K_1/C_S in equation (3.16) is monotonically increasing through a zero value as $\mathscr{T}$ increases. Specifically, we find that when $\mathscr{T} < 3 + 2\sqrt{3} \approx 6.464$, the bifurcation to convection with upflow at the centres of distorted hexagons is subcritical, whereas when

$$\mathscr{T} > 3 + 2\sqrt{3}, \tag{4.12}$$

supercritical bifurcation arises.

Figure 6 displays a bifurcation diagram for three-dimensional distorted hexagons. The diagram is shown for two values of $\mathscr{T}$, corresponding to initially subcritically (the

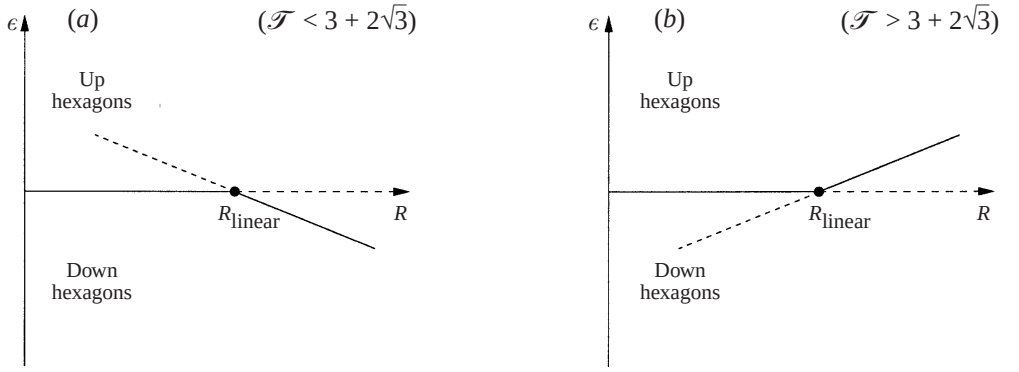

FIGURE 6. Bifurcation diagram for three-dimensional distorted hexagons. As in figure 3, the amplitude of the nonlinear perturbations, ϵ, is plotted *vs.* Rayleigh number, R, for two cases. The value R_{linear} corresponds to the linear critical Rayleigh number given by $R_{\text{linear}} = R_{0c} + \delta R_{1\delta} + O(\delta^2)$. Solid and dashed curves represent the presumed stable and unstable portions of the solution branches, respectively. The portions of the branches with $\epsilon > 0$ ($\epsilon < 0$) correspond to hexagons with upflow (downflow) at the centres. (*a*) The case when $\mathscr{T} < 3 + 2\sqrt{3}$, and (*b*) the case when $\mathscr{T} > 3 + 2\sqrt{3}$. Notice that it is the rotational constraint of the system which allows the possibility of initially supercritical up-hexagons.

case when $\mathscr{T} < 3 + 2\sqrt{3}$, figure 6*a*) and supercritically (the case when $\mathscr{T} > 3 + 2\sqrt{3}$, figure 6*b*) bifurcating distorted hexagons with upflow at their centres.

The same kind of qualitative argument to explain the effect of rotation at finite amplitudes as that presented in the previous subsection on rolls can be used in connection with hexagons. Thus it is possible that hexagonal convection with finite amplitude may exist at supercritical values of the Rayleigh number because the Coriolis force may balance the destabilizing effect associated with the nonlinear effective viscous dissipation in the porous medium.

We close the discussion of the solvability condition for the hexagonal solution by identifying the maximum allowed value of the perturbation amplitude ϵ for the theory to be valid. Again, as in the case of oblique rolls, we compare the basic-state solid fraction with its perturbation given by (3.13*b*) and find

$$\epsilon_{\max}(\mathscr{T}) = \frac{\delta}{6\pi(\sqrt{\mathscr{T}+1}+1)} + O(\delta^2), \tag{4.13}$$

which is 1/3 times that required for rolls.

4.3. *Relationship to experiments*

The particular phenomenon we are concerned with in this paper occurs when convection in the mushy layer does not become too vigorous. Therefore, although the results of this paper are indicative of a tendency to suppress the local remelting of dendrites in the rotating mushy layer, no such conclusion about the effect of rotation can clearly be inferred from the present study for convective states in which the chimneys are fully developed. Note that in the model we analyse here, and in all the linear and weakly nonlinear analyses to date, there is no chimney *per se*; just a region of reduced local solid fraction at the upflowing centres of convection cells.

Only one experimental study has been reported relating to weak convection in a non-rotating mushy layer (Tait, Jahrling & Jaupart 1992). By slow cooling and solidifying of an ammonium chloride solution, they were able to observe the planform of chimney convection near the onset of critical convection. The planform was

statistically closest to a hexagonal pattern with upflow along the edges and downflow at the centres of hexagons. This observed phenomenon is in contrast with theoretical results of Amberg & Homsy (1993), in which it was anticipated that hexagons with upflow at the centres would be stable. Anderson & Worster (1995) gave some possible explanations for this discrepancy by studying the additional physical effects and interactions within the model of Amberg & Homsy. Specifically, their results suggested that, under certain conditions, hexagons with downflow at the centres can be stable and first to occur, as observed in the experiments by Tait *et al.* (1992).

Although the plausibility in relation to existing experimental results of the mushy layer model proposed by Amberg & Homsy (1993), and used also in the present analysis, is restricted for a variety of reasons, including the dynamical isolation of the mushy layer from the overlying liquid region and the prescribed constrained growth at constant solidification rate, the qualitative rather than quantitative predictions associated with this model are of value, as discussed by Anderson & Worster (1995, 1996).

To date, all reported experimental observations of rotating convection in mushy layers (Sample & Hellawell 1982, 1984; Claßen *et al.* 1999) have concentrated on strongly nonlinear convection with fully developed chimneys, rather than the weak convection that we require, so the effects of rotation of the type described in this paper, most notably the suppression of the nascent chimneys in the interior of the mushy layer, have not been reported. It is only in the near-critical situation that the qualitative results of the present study should be robust and experimentally observed. Clearly, more detailed and careful experiments, similar to those by Tait *et al.* (1992), in which disturbances are controlled using a much lower cooling rate than in the experiments by Sample & Hellawell (1982, 1984) and Claßen *et al.* (1999), are needed to make specific comparisons with predictions resulting from the present study.

In general, an $O(1)$ value for the square root of the Taylor number is required in order for the qualitative effects of rotation revealed by our analysis to be present in an experimental situation. For the ammonium-chloride–water system, we have already shown that this limiting case can be achieved by values of the angular velocity about $2\,\mathrm{rad\,s^{-1}}$, which are quite accessible in the laboratory. In metal alloys the typical values of permeability are generally much lower than the values in aqueous solutions of ammonium chloride; for the Pb–Sn alloy system, for example, if we assume $\Pi(0) = 1.6 \times 10^{-5}\,\mathrm{cm^2}$ and $\nu = 0.25 \times 10^{-2}\,\mathrm{cm^2\,s^{-1}}$ (Sarazin & Hellawell 1988) then an angular velocity of about $80\ \mathrm{rad\,s^{-1}}$ is required in order for $\sqrt{\mathscr{T}} = O(1)$. Hence, the metal alloys (under laboratory conditions) may not be a convenient candidate to exhibit the effects predicted by the present work.

However, the study of rotating convection in mushy layers presented in this paper is not motivated only by possible practical applications in industrial casting processes. A further motivation is the solidification and convective dynamics of the Earth's core (Loper & Roberts 1981; Fearn, Loper & Roberts 1981; Fearn 1998). It is thought that the Earth's core is an iron-rich alloy of iron and a light constituent, perhaps sulphur or oxygen. The thermodynamic conditions are such that a freezing interface between the solid inner core and the liquid outer core is not sharp; the inner core may grow dendritically, and the mushy state may extend to the Earth's centre (Fearn *et al.* 1981). Using an estimate of the dendrite spacing in the core deduced from meteorites (Esbensen & Buchwald 1982), Bergman & Fearn (1994) estimated the permeability to be $1\,\mathrm{m^2}$. This can result in a large value of the Taylor number appropriate to the Earth's inner core; assuming a fluid molecular viscosity of $10^{-6}\,\mathrm{m^2\,s^{-1}}$ (Stacey 1992) and an angular velocity of $7 \times 10^{-5}\ \mathrm{rad\,s^{-1}}$, we estimate the value of $\sqrt{\mathscr{T}}$ to be

larger than the $O(1)$ value required in the present analysis by two orders of magnitude. Therefore, it is of considerable geophysical interest to investigate the effects of rotation on the convective flow generated within the mushy zone at the inner-core boundary, although it should be emphasized that this large-scale solidifying system may be far from eutectic, contrary to what is assumed herein.

5. Conclusion

In this contribution, we have analysed the effects of an imposed rotational constraint on the onset of instability to infinitesimal steady convection as well as on the onset of finite-amplitude steady motions in a rotating mushy layer. We have used a simple physical model of the mushy layer proposed by Amberg & Homsy (1993) in which the mushy layer is physically isolated from the underlying solid and overlying liquid regions. We have extended this original mushy-layer model to the case in which the system is in a state of uniform rotation about the vertical.

Perhaps the most important results in our linear stability investigation are the two following. First, we have found that the increase in the Taylor number $\mathscr{T}$, which is proportional to the uniform angular velocity of the system, tends primarily to increase the linear, critical Rayleigh number, and therefore causes the system to be more stable. This is because the rotation of the system introduces a solutal wind balance in which the horizontal concentration gradient can be, at least partly, balanced by the vertical shear of the zonal component of the flow. In terms of energy, the destabilizing potential energy available to a disturbed fluid element partially contributes to the zonal velocity field of that element. This becomes more and more pronounced as $\mathscr{T}$ increases and is the principal reason for the inhibition of compositional convection in the rotating mushy layer. Such behaviour is similar to the linear aspects of the stability problem of steady Boussinesq Bénard convection in a rotating fluid layer.

Second, in addition to its more familiar stabilizing role, the presence of the rotational constraint can be accompanied by a qualitative change in the physical effects which are intrinsic to the mushy layer and which are included in the analysis as perturbations to the near-eutectic approximation of the system. In particular, analysing the first-order correction to the linear, critical Rayleigh number, we have discovered that the stabilizing effect of increasing the linear measure of permeability variations, K_1, is constrained to the range $0 \leqslant \mathscr{T} < 3$ of Taylor numbers. Once $\mathscr{T}$ is increased through this range, increasing K_1 can no longer stabilize the system. This striking and unsuspected feature of the rotating, solidifying, reactive porous medium can be traced to the momentum balance appearing at $O(\epsilon^1)$. Physically, as the permeability coefficient K_1 increases, the resistance to flow increases correspondingly, leading to a decrease in the solutal wind flow for a given value of the Taylor number $\mathscr{T}$ and therefore making the system linearly more unstable.

The analysis of this paper has also revealed interesting and important results regarding the nonlinear aspects of rotating convection in the mushy layer. In particular, we have identified steady solutions to our weakly nonlinear rotating system in the form of two-dimensional oblique rolls and of three-dimensional convection with hexagonal symmetry. The two-dimensional oblique rolls were found to be either subcritically or supercritically bifurcating; an analytical expression for the transition from subcritical to supercritical rolls has been obtained in terms of the parameter combination K_1/C_S *vs.* Taylor number $\mathscr{T}$ provided $K_2 = 0$. Three-dimensional convection with hexagonal symmetry was found to be, in general, transcritical. Note that in the non-rotating system studied by Amberg & Homsy (1993) the regular hexagons

were also transcritically bifurcating. Moreover, the nature of this bifurcation cannot change in the non-rotating system. In the rotating system we have been concerned with here, however, the nature of the transcritical bifurcation can vary, depending crucially on the value of the Taylor number $\mathscr{T}$. As a result, both subcritical and supercritical bifurcations with upflow at the centres of distorted hexagons can become possible. According to the results of our finite-amplitude study, the rotational constraint imposed on the solidifying system minimizes the tendency to subcriticality of both the bifurcation to oblique rolls and distorted hexagons with upflow at the centres, and hence presumably causes these states to become nonlinearly more stable.

It should, of course, be remembered that the results of the present analysis cannot be extended right up to $\sqrt{\mathscr{T}} \gg 1$. We expect, however, that the asymptotic limit that we have chosen in the present work ($\delta \to 0$, $\sqrt{\mathscr{T}} = O(1)$) is representative in all qualitative aspects regarding the nature of the onset of infinitesimal instability as well as finite-amplitude convection in the rotating mushy layer.

We have made preliminary calculations using a model of a mushy layer that includes the variation of the local solid fraction in the Coriolis term (cf. the definition of the Taylor number (2.5*d*)) to test the robustness of the results revealed by the present analysis. Specifically, we calculated the parametric trends in terms of the boundary between subcritical and supercritical bifurcations. The results indicate that, although the parametric trends quantitatively differ from those in the present paper (i.e. figure 2 and equation (4.12)), they have the same topology and also give way to supercritically bifurcating oblique rolls and up-hexagons at larger values of the Taylor number $\mathscr{T}$ – the result which is perhaps the most important consequence of the present study.

Although the quantitative conclusions of the present study are not directly applicable to the experimental situation, the qualitative results we have discovered are of value. Unfortunately, unlike for the non-rotating case, there exists, to our knowledge, no reported experimental observation for the onset of near-critical convection in the rotating mushy layer, to which the details of the present model near the bifurcation point could be compared. It is hoped therefore that the richness of predictions resulting from the present study might provide a stimulation for experimental verification of its range of validity.

This work was improved during my visit to DAMTP, University of Cambridge. I am very indebted to M. G. Worster for his hospitality, and for numerous stimulating discussions during this visit. I am grateful to D. M. Anderson for helpful comments on an earlier draft of this paper. Thanks are also due to J. Bod'a for introducing me to the problem of convection in mushy layers, and S. Ševčík who continually encouraged me to complete this investigation.

Appendix

Writing, for brevity

$$l(\mathscr{T}) = 1 + \exp\left[\pi(\mathscr{T} + \sqrt{\mathscr{T}+1} + 2)^{1/2}(\mathscr{T}+1)^{-1/4}\right], \tag{A 1a}$$

$$m(\mathscr{T}) = \frac{192}{\pi} l(\mathscr{T})[-2 + l(\mathscr{T})]^{-1}\mathscr{T}^2(\mathscr{T}+1)^{3/4}(\sqrt{\mathscr{T}+1}+1)^3(\mathscr{T}+\sqrt{\mathscr{T}+1}+2)^{1/2}, \tag{A 1b}$$

$$1/n(\mathscr{T}) = 96\pi\sqrt{\mathscr{T}+1}(\sqrt{\mathscr{T}+1}+1)^{12}, \tag{A 1c}$$

the expressions for the functions of Taylor number $\mathscr{T}$ appearing in equation (3.10*a*) have the following forms:

$$a(\mathscr{T}) = -\frac{1}{12\pi}\frac{6\mathscr{T} + [\mathscr{T}(3+2\pi^2) - 4\pi^2]\sqrt{\mathscr{T}+1} - 4\pi^2}{\sqrt{\mathscr{T}+1}(\sqrt{\mathscr{T}+1}+1)}, \tag{A 2a}$$

$$b(\mathscr{T}) = \left(\frac{\pi}{4} + \frac{2}{\pi}\right)(\sqrt{\mathscr{T}+1}+1), \tag{A 2b}$$

$$\begin{aligned} c(\mathscr{T}) = &-(\mathscr{T}+1)^{-1} n(\mathscr{T})\{(\mathscr{T}+3)^2 m(\mathscr{T}) + \mathscr{T}^8(10\pi^2+21) \\ &+\mathscr{T}^7[2\pi^2(67\sqrt{\mathscr{T}+1}+448) + 3(87\sqrt{\mathscr{T}+1}+518)] \\ &+\mathscr{T}^6[2\pi^2(1957\sqrt{\mathscr{T}+1}+6573) + 3(2067\sqrt{\mathscr{T}+1}+6399)] \\ &+4\mathscr{T}^5[\pi^2(8055\sqrt{\mathscr{T}+1}+18037) + 12(897\sqrt{\mathscr{T}+1}+1891)] \\ &+16\mathscr{T}^4[\pi^2(6907\sqrt{\mathscr{T}+1}+11507) + 3(2679\sqrt{\mathscr{T}+1}+4331)] \\ &+64\mathscr{T}^3[\pi^2(2699\sqrt{\mathscr{T}+1}+3517) + 6(485\sqrt{\mathscr{T}+1}+637)] \\ &+2304\mathscr{T}^2[46\pi^2(\sqrt{\mathscr{T}+1}+1) + (53\sqrt{\mathscr{T}+1}+57)] \\ &+1024\mathscr{T}[-5\pi^2(\sqrt{\mathscr{T}+1}+3) + 3(5\sqrt{\mathscr{T}+1}+3)] \\ &+4096[-5\pi^2(\sqrt{\mathscr{T}+1}+1) - 3(\sqrt{\mathscr{T}+1}+1)]\}, \end{aligned} \tag{A 2c}$$

$$d(\mathscr{T}) = -\frac{\pi}{8}\frac{(\sqrt{\mathscr{T}+1}+1)(\sqrt{\mathscr{T}+1}-2)}{\sqrt{\mathscr{T}+1}}, \tag{A 2d}$$

$$\begin{aligned} e(\mathscr{T}) = &\, n(\mathscr{T})\{(\mathscr{T}+1)m(\mathscr{T}) + \mathscr{T}^7(\pi^2-3) \\ &+\mathscr{T}^6[\pi^2(17\sqrt{\mathscr{T}+1}+129) - 3(13\sqrt{\mathscr{T}+1}+113)] \\ &+16\mathscr{T}^5[19\pi^2(2\sqrt{\mathscr{T}+1}+7) - 6(17\sqrt{\mathscr{T}+1}+58)] \\ &+16\mathscr{T}^4[\pi^2(337\sqrt{\mathscr{T}+1}+769) - 3(281\sqrt{\mathscr{T}+1}+613)] \\ &+64\mathscr{T}^3[\pi^2(303\sqrt{\mathscr{T}+1}+517) - 6(113\sqrt{\mathscr{T}+1}+185)] \\ &+768\mathscr{T}^2[\pi^2(43\sqrt{\mathscr{T}+1}+59) - (85\sqrt{\mathscr{T}+1}+113)] \\ &+1024\mathscr{T}[2\pi^2(13\sqrt{\mathscr{T}+1}+15) - 3(15\sqrt{\mathscr{T}+1}+17)] \\ &+4096[2\pi^2(\sqrt{\mathscr{T}+1}+1) - 3(\sqrt{\mathscr{T}+1}+1)]\}, \end{aligned} \tag{A 2e}$$

$$f(\mathscr{T}) = \frac{3}{8}\pi(\sqrt{\mathscr{T}+1}+1), \tag{A 2f}$$

$$\begin{aligned} h(\mathscr{T}) = &-2n(\mathscr{T})\{(\mathscr{T}+3)m(\mathscr{T}) + \mathscr{T}^7(\pi^2-9) \\ &+\mathscr{T}^6[\pi^2(11\sqrt{\mathscr{T}+1}+51) - 3(33\sqrt{\mathscr{T}+1}+197)] \\ &+8\mathscr{T}^5[2\pi^2(7\sqrt{\mathscr{T}+1}+2) - 3(85\sqrt{\mathscr{T}+1}+207)] \\ &+16\mathscr{T}^4[-\pi^2(53\sqrt{\mathscr{T}+1}+213) - 3(143\sqrt{\mathscr{T}+1}+131)] \\ &+64\mathscr{T}^3[-\pi^2(131\sqrt{\mathscr{T}+1}+265) + 6(25\sqrt{\mathscr{T}+1}+89)] \\ &+256\mathscr{T}^2[-5\pi^2(17\sqrt{\mathscr{T}+1}+25) + 3(87\sqrt{\mathscr{T}+1}+139)] \\ &+1024\mathscr{T}[-2\pi^2(11\sqrt{\mathscr{T}+1}+13) + 3(29\sqrt{\mathscr{T}+1}+35)] \\ &+4096[-2\pi^2(\sqrt{\mathscr{T}+1}+1) + 9(\sqrt{\mathscr{T}+1}+1)]\}. \end{aligned} \tag{A 2g}$$

REFERENCES

Amberg, G. & Homsy, G. M. 1993 Nonlinear analysis of buoyant convection in binary solidification with application to channel formation. *J. Fluid Mech.* **252**, 79–98.

Anderson, D. M. & Worster, M. G. 1995 Weakly nonlinear analysis of convection in mushy layers during the solidification of binary alloys. *J. Fluid Mech.* **302**, 307–331.

Anderson, D. M. & Worster, M. G. 1996 A new oscillatory instability in a mushy layer during the solidification of binary alloys. *J. Fluid Mech.* **307**, 245–267.

Bergman, M. I. & Fearn, D. R. 1994 Chimneys on the Earth's inner–outer core boundary? *Geophys. Res. Lett.* **21**, 477–480.

Busse, F. H. 1967 The stability of finite amplitude cellular convection and its relation to an extremum principle. *J. Fluid Mech.* **30**, 625–649.

Chandrasekhar, S. 1961 *Hydrodynamic and Hydromagnetic Stability*. Clarendon.

Chen, C. F. & Chen, F. 1991 Experimental study of directional solidification of aqueous ammonium chloride solution. *J. Fluid Mech.* **227**, 567–586.

Claßen, S., Heimpel, M. & Christensen, U. 1999 Blob instability in rotating compositional convection. *Geophys. Res. Lett.* **26**, 135–138.

Copley, S. M., Giamei, A. F., Johnson, S. M. & Hornbecker, M. F. 1970 The origin of freckles in unidirectionally solidified castings. *Metall. Trans.* **1**, 2193–2204.

Emms, P. W. & Fowler, A. C. 1994 Compositional convection in the solidification of binary alloys. *J. Fluid Mech.* **262**, 111–139.

Esbensen, K. H. & Buchwald, V. F. 1982 Planet(oid) core crystallization and fractionation-evidence from the Apaghlik mass of the Cape York iron meteorite shower. *Phys. Earth Planet. Inter.* **29**, 218–232.

Fearn, D. R. 1998 Hydromagnetic flow in planetary cores. *Rep. Prog. Phys.* **61**, 175–235.

Fearn, D. R., Loper, D. E. & Roberts, P. H. 1981 Structure of the Earth's inner core. *Nature* **292**, 232–233.

Fowler, A. C. 1985 The formation of freckles in binary alloys. *IMA J. Appl. Maths* **35**, 159–174.

Guba, P. & Bod'a, J. 1998 The effect of uniform rotation on convective instability of a mushy layer during binary alloys solidification. *Studia Geoph. et Geod.* **42**, 289–296.

Loper, D. E. & Roberts, P. H. 1981 A study of conditions at the inner-core boundary of the Earth. *Phys. Earth Planet. Inter.* **24**, 302–307.

Malkus, W. V. R. & Veronis, G. 1958 Finite amplitude cellular convection. *J. Fluid Mech.* **4**, 225–260.

Manneville, P. 1990 *Dissipative Structures and Weak Turbulence*. Academic.

Nield, D. A. 1999 Modeling the effects of a magnetic field or rotation on flow in a porous medium: momentum equation and anisotropic permeability analogy. *Intl J. Heat Mass Transfer* **42**, 3715–3718.

Nield, D. A. & Bejan, A. 1999 *Convection in Porous Media*. Springer.

Palm, E. & Tyvand, A. 1984 Thermal convection in a rotating porous layer. *Z. Angew. Math. Phys.* **35**, 122–123.

Palm, E., Weber, J. E. & Kvernvold, O. 1972 On steady convection in a porous medium. *J. Fluid Mech.* **54**, 153–161.

Porter, D. A. & Easterling, K. E. 1992 *Phase Transformations in Metals and Alloys*. Chapman & Hall.

Sample, A. K. & Hellawell, A. 1982 The effect of mold precession on channel and macro-segregation in ammonium chloride–water analog castings. *Metall. Trans.* B **13**, 495–501.

Sample, A. K. & Hellawell, A. 1984 The mechanisms of formation and prevention of channel segregation during alloy solidification. *Metall. Trans.* A **15**, 2163–2173.

Sarazin, J. R. & Hellawell, A. 1988 Channel formation in Pb–Sn, Pb–Sb, and Pb–Sn–Sb alloy ingots and comparison with the system NH_4Cl–H_2O. *Metall. Trans.* A **19**, 1861–1871.

Stacey, F. D. 1992 *Physics of the Earth*. Brookfield.

Tait, S., Jahrling, K. & Jaupart, C. 1992 The planform of compositional convection and chimney formation in a mushy layer. *Nature* **359**, 406–408.

Tait, S. & Jaupart, C. 1992 Compositional convection in a reactive crystalline mush and melt differentiation. *J. Geophys. Res.* **97**(B5), 6735–6756.

VADASZ, P. 1998*a* Coriolis effect on gravity-driven convection in a rotating porous layer heated from below. *J. Fluid Mech.* **376**, 351–375.

VADASZ, P. 1998*b* Flow in rotating porous media. In *Fluid Transport in Porous Media* (ed. J. P. Du Plessis), chapter 4. Computational Mechanics Publications, Southampton: WIT Press.

VERONIS, G. 1959 Cellular convection with finite amplitude in a rotating fluid. *J. Fluid Mech.* **5**, 401–435.

WORSTER, M. G. 1992 Instabilities of the liquid and mushy regions during solidification of alloys. *J. Fluid Mech.* **237**, 649–669.

WORSTER, M. G. 1997 Convection in mushy layers. *Ann. Rev. Fluid Mech.* **29**, 91–122.